

Stability analysis of transversely isotropic laminated Mindlin plates with piezoelectric layers using a Levy-type solution

M.A. Ghasemabadian^{1a} and A.R. Saidi^{*2}

¹Department of Mechanical Engineering, Ferdowsi University of Mashhad, Mashhad, Iran

²Department of Mechanical Engineering, Shahid Bahonar University of Kerman, Kerman, Iran

(Received February 14, 2016, Revised October 21, 2016, Accepted November 23, 2016)

Abstract. In this paper, based on the first-order shear deformation plate theory, buckling analysis of piezoelectric coupled transversely isotropic rectangular plates is investigated. By assuming the transverse distribution of electric potential to be a combination of a parabolic and a linear function of thickness coordinate, the equilibrium equations for buckling analysis of plate with surface bonded piezoelectric layers are established. The Maxwell's equation and all boundary conditions including the conditions on the top and bottom surfaces of the plate for closed and open circuited are satisfied. The analytical solution is obtained for Levy type of boundary conditions. The accurate buckling load of laminated plate is presented for both open and closed circuit conditions. From the numerical results it is found that, the critical buckling load for open circuit is more than that of closed circuit in all boundary and loading conditions. Furthermore, the critical buckling loads and the buckling mode number increase by increasing the thickness of piezoelectric layers for both open and closed circuit conditions.

Keywords: buckling; piezoelectric; rectangular plate; transversely isotropic; analytical solution

1. Introduction

The growth of researches on piezoelectric rectangular plates and beams in general has evolved during past decade in part by focusing on free and forced vibration, buckling and post-buckling, dynamic and static stability analysis.

Among various researches on the buckling and post buckling analysis of piezoelectric beams, using classical beam theory, De Faria and De Almeida (1999) reported a theoretical framework and a finite element for the buckling of beams with a pair of surface attached piezoactuators, and presented the enhancement of prebuckling behavior of slender beams through piezoelectric control. The elastic buckling of a column structure with a pair of piezoelectric layers was presented by Wang (2002). He found that, by designing optimal location of the piezoelectric layer and the voltage applied to the piezoelectric layers, the buckling capacity of the column structure could be enhanced effectively. Wang and Quek (2002) showed the effectiveness of a pair of surface-bonded piezoelectric patches on increasing the buckling capacity of a column subjected to a follower force. De Faria (2004) proposed a new way of increasing the buckling capability of composite columns. For buckling analysis of hybrid piezoelectric beams under electromechanical loads, a coupled one-dimensional geometrically nonlinear zigzag theory was developed by Kapuria and Alam (2004a). Also, they

(2004b) presented a two-dimensional exact solution for buckling of simply supported symmetrically laminated hybrid beam and cross-ply panel with elastic substrate and piezoelectric layers. With the help of finite element method, buckling behavior of smart beams and plates under different electrical conditions as well as thermal and electrical loading was presented by Giannopoulos *et al.* (2007). Cheng *et al.* (2008) showed that applying the adaptive control of electric field to the surface bonded piezoelectric patch lead to decrease the lateral deflection of laminated composite beam and increase its dynamic buckling capacity. Jerome and Ganesan (2010) developed a new two dimensional plane strain finite element formulation to predict the critical buckling load of a piezocomposite beam. They presented the results for both open and closed circuit electrical conditions. Wang (2010) studied the application of using piezoelectric actuators and strain gauge sensors to control the buckling of both simply supported and cantilever beams based on finite element method.

In the same manner, buckling and postbuckling analysis of piezoelectric plates, have been investigated by many researchers. Several works have been conducted to investigate the buckling, postbuckling and thermal buckling behaviors of smart composite plates. For instance, on the basis of first order shear deformation plate theory, Chandrashekhara and Bathia (1993) developed a finite element model for active buckling control of laminated composite plates using piezoelectric materials. Considering large thermopiezoelectric deflections, Postbuckling and vibration analysis of fully symmetric and partially eccentric piezolaminated composite plates were carried out by Oh *et al.* (2000). For fully distributed piezolaminates, their study showed that excessive bending moments for the suppression of thermally buckled deflection may cause another type of

*Corresponding author, Professor

E-mail: saidi@uk.ac.ir

^aPh.D. Student

E-mail: ghasemabadian@stu.um.ac.ir

structural instability. Based on the classical plate theory with von-Karman nonlinear kinematic relations, Tang (2016) developed an analytical solution to investigate the thermal buckling behavior of the imperfect rectangular plates with functionally graded (FG) coatings under uniform temperature rise. Lei *et al.* (2016) studied the buckling behavior of carbon nanotube reinforced functionally graded (CNTR-FG) composite laminated plates based on the first-order shear deformation theory and using meshless kp-Ritz method. Thai *et al.* (2014) presented a new first-order shear deformation theory for functionally graded sandwich plates composed of functionally graded face sheets and an isotropic homogeneous core. By making a further assumption to the existing first-order shear deformation theory, they reduced the number of unknowns and governing equations of the present theory. Based on the higher order shear deformation plate theory, thermal postbuckling and postbuckling analysis of a simply supported laminated plate with piezoelectric actuators subjected to thermo-electrical and thermo-electro-mechanical loads were presented by Shen (2001a, b). A numerical analysis for dynamic buckling of a plate with surface bonded piezoceramic elements was presented by Batra and Geng (2001a) based on the three dimensional elasticity theory. In that work, the geometric and material nonlinearity of the structures were taken into account. They found that an increase in the plate thickness relative to that of the piezoelectric layers decreases its effectiveness in enhancing the buckling load of the plate. Varelis and Saravanos (2002) studied the static buckling control of smart beams and plates. The buckling and postbuckling response of composite laminates and plates with piezoactuators and sensors due to large displacements and rotations has been presented by Varelis and Saravanos (2004). Their results indicate that, depending on the applied field polarity, mechanical buckling maybe either compensated or promoted. Kapuria and Achary (2004) presented a three dimensional exact piezoelectricity solution for buckling of simply-supported symmetrically laminated hybrid plates with elastic substrate and piezoelectric layers. Kapuria and Achary (2006) developed a coupled zigzag theory for static buckling analysis of hybrid piezoelectric plates. Using three dimensional state-space formulations, the buckling of simply supported orthotropic piezoelectric laminates with weak interfaces was investigated by Kim and Lee (2008). Dynamic buckling of laminated plates with piezoelectric sensors and actuators under thermo-electro-mechanical loadings was studied by Shariyat (2009a). Using the piezoelectric elements, De Faria and Donadon (2010) proposed a technique for increasing the buckling loads of composite plates. Three dimensional thermal buckling analysis of piezoelectric antisymmetric angle-ply laminates using finite layer method has been done by Akhras and Li (2010).

Some authors have studied the piezoelectricity effects on the buckling and postbuckling behavior of functionally graded (FG) plates with piezoelectric layers. The postbuckling behavior of piezoelectric FG plates subjected to thermo-electro-mechanical loading was presented by Liew *et al.* (2003). They reported that the buckling and

postbuckling strength of plate can be improved by application of negative voltage in the actuator layers. Shen (2005) studied the postbuckling analysis of simply supported, symmetric FG plates with fully covered or embedded piezoelectric actuators subjected to the thermo-electro-mechanical loads. Based on higher order shear deformation plate theory, forced and free vibration and dynamic buckling of rectangular FG plates with piezoelectric sensors and actuators subjected to thermo-electro-mechanical loading conditions were investigated by Shariyat (2009b). His results revealed that the natural frequencies and the thermal and mechanical buckling loads were slightly higher when a minus control voltage was used. Shen (2009) presented a fully nonlinear postbuckling and thermal postbuckling analysis for FG hybrid plates with PFRC actuators. Thermal buckling analysis of FG plates with piezoelectric actuators subjected to thermo-electrical loadings was presented by Mirzavand and Eslami (2011). Recently the stability analysis of a functionally graded plate integrated with a piezoelectric sensor and actuator at the top and bottom faces subjected to electrical and mechanical loading was investigated by Jadhav and Bajoria (2012). They used finite element method and solved the problem for simply supported and clamped boundary conditions. Abdollahi *et al.* (2015) investigated the buckling analysis of thick functionally graded piezoelectric rectangular plates based on the higher-order shear and normal deformable plate theory. They considered two cases consisting of open-closed and closed circuits as electrical conditions. Yaghoobi and Rajabi (2013) presented an analytical method to analyze the buckling of piezoelectric coupled plates with different boundary conditions on the basis of the first order shear deformation plate theory. Also, Chen *et al.* (2008) investigated the buckling of piezoelectric functionally graded material with the element free Galerkin method. Finally, Arefi (2016) studied mechanical stability of the functionally graded rectangular plates bonded with functionally graded piezoelectric layers based on Classical plate theory.

They used finite element method and solved the problem for simply supported and clamped boundary conditions. Finally, Abdollahi *et al.* (2015) investigated the buckling analysis of thick functionally graded piezoelectric rectangular plates based on the higher-order shear and normal deformable plate theory. They considered two cases consisting of open-closed and closed circuits as electrical conditions.

According to the all-around literature review it can be found that there is no analytical studying on the buckling analysis of a rectangular plate embedded by piezoelectric layers even for isotropic materials which consider Levy type boundary conditions as mechanical boundary conditions and open and closed circuit conditions as electrical surface conditions and Maxwell equation as an extra equation and assume a combination of a parabolic and a linear function of thickness for transverse distribution of electric potential. In this work, based on the first-order shear deformation theory, buckling analysis of a transversely isotropic rectangular plate embedded by piezoelectric layers is done for both open and closed

circuited electrical conditions. In order to satisfy the Maxwell's equation and all electrical boundary conditions including the conditions on the top and bottom surfaces of the plate for closed and open circuited, it is assumed that the function of electric potential is a combination of parabolic and linear functions of thickness coordinate z . Employing the principle of minimum total potential energy, the equilibrium equations of above mentioned plate are derived.

In order to present an analytical solution for rectangular plates, there are two well-known boundary conditions, the first one is Navier type boundary condition (all edges simply supported) and the second one is Levy type boundary condition (plates with at least two opposite edges simply supported and remaining ones arbitrary, including free, simple support, or fixed support). It is mentioned that Levy type boundary condition is more generic than Navier one. Furthermore, the idea of Levy-type method can be used for various boundary conditions to reduce the governing partial differential equations to a system of ordinary ones which may be solved exactly. Therefore, by using Levy-type solution and two auxiliary functions, four coupled governing partial differential equations are decoupled into two decoupled partial differential equations. The accurate critical buckling load is obtained for Levy-type boundary conditions. Revealing the accuracy of the present solution, a comparison is done for a special case of isotropic plate without piezoelectric layers. Finally, the effects of aspect ratio, piezoelectric thickness, plate thickness, boundary conditions, loading conditions for some different piezoelectric materials are comprehensively investigated.

2. Stability equations

Consider a flat rectangular plate as shown in Fig. 1 consisting of a host layer and two piezoelectric layers with the length a , width b , host layer thickness $2h$ and piezoelectric layer thickness h_p . Both piezoelectric layers are polarized perpendicular to the mid-plane in the direction of the z -axis. The host layer is made of transversely isotropic material where the xy -plane is the plane of isotropy.

The displacement components of the plate based on the first-order shear deformation plate theory (FSDT) are considered as

$$\begin{aligned} U_1(x, y, z) &= u(x, y) + z\psi_x(x, y) \\ U_2(x, y, z) &= v(x, y) + z\psi_y(x, y) \\ U_3(x, y, z) &= w(x, y) \end{aligned} \tag{1}$$

where z is the thickness coordinate, u and v are the mid-plane displacement of the plate in the x and y directions, respectively, w is the transverse displacement and ψ_x and ψ_y are rotation functions of mid-plane. Considering the Von-Karman hypothesis, the nonlinear form of strain components are stated as

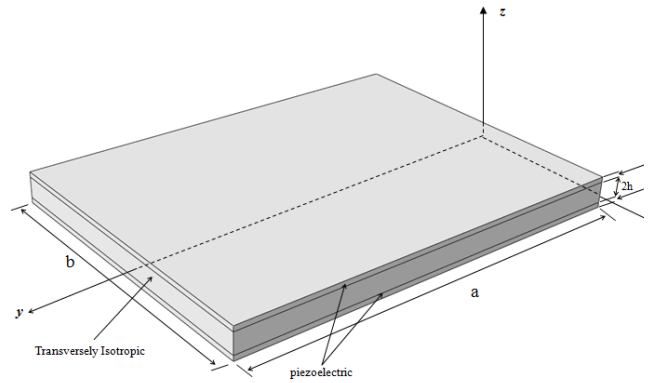


Fig. 1 The geometry and coordinate of a piezoelectric coupled rectangular plate

$$\begin{pmatrix} \epsilon_{xx} \\ \epsilon_{yy} \\ \gamma_{xy} \\ \gamma_{xz} \\ \gamma_{yz} \end{pmatrix} = \begin{pmatrix} \epsilon_1 \\ \epsilon_2 \\ \epsilon_3 \\ \epsilon_4 \\ \epsilon_5 \end{pmatrix} + z \begin{pmatrix} \kappa_1 \\ \kappa_2 \\ \kappa_3 \\ \kappa_4 \\ \kappa_5 \end{pmatrix} \tag{2a}$$

$$\begin{pmatrix} \epsilon_1 \\ \epsilon_2 \\ \epsilon_3 \\ \epsilon_4 \\ \epsilon_5 \end{pmatrix} = \begin{pmatrix} u_{,x} + w_{,x}^2 / 2 \\ v_{,y} + w_{,y}^2 / 2 \\ u_{,y} + v_{,x} + w_{,x}w_{,y} \\ \psi_x + w_{,x} \\ \psi_y + w_{,y} \end{pmatrix} \tag{2b}$$

$$\begin{pmatrix} \kappa_1 \\ \kappa_2 \\ \kappa_3 \\ \kappa_4 \\ \kappa_5 \end{pmatrix} = \begin{pmatrix} \psi_{x,x} \\ \psi_{y,y} \\ \psi_{x,y} + \psi_{y,x} \\ 0 \\ 0 \end{pmatrix} \tag{2c}$$

where the subscript (,) denotes derivation with respect to the corresponding coordinates.

The stress components in the host plate are expressed as

$$\begin{Bmatrix} \sigma_{xx}^h \\ \sigma_{yy}^h \\ \sigma_{xy}^h \\ \sigma_{xz}^h \\ \sigma_{yz}^h \end{Bmatrix} = \begin{bmatrix} E & \nu E & 0 & 0 & 0 \\ 1-\nu^2 & 1-\nu^2 & 0 & 0 & 0 \\ \nu E & E & 0 & 0 & 0 \\ 1-\nu^2 & 1-\nu^2 & 0 & 0 & 0 \\ 0 & 0 & \frac{E}{2(1+\nu)} & 0 & 0 \\ 0 & 0 & 0 & K^2 G_z & 0 \\ 0 & 0 & 0 & 0 & K^2 G_z \end{bmatrix} \begin{Bmatrix} \epsilon_{xx} \\ \epsilon_{yy} \\ \gamma_{xy} \\ \gamma_{xz} \\ \gamma_{yz} \end{Bmatrix} \tag{3}$$

in which the superscript (*h*) represents the variable in the host structure. Furthermore, K^2 which is the shear correction factor employed in Mindlin's plate model to correct the shear stress in thickness direction, is chosen as 5/6. Furthermore, G_z is the shear modulus in the plane of isotropy which is generally different from $E/2(1+\nu)$.

The stress components in the piezoelectric layer can be written as

$$\begin{Bmatrix} \sigma_{xx}^p \\ \sigma_{yy}^p \\ \sigma_{xy}^p \\ \sigma_{xz}^p \\ \sigma_{yz}^p \end{Bmatrix} = \begin{bmatrix} \bar{C}_{11}^E & \bar{C}_{12}^E & 0 & 0 & 0 \\ \bar{C}_{12}^E & \bar{C}_{11}^E & 0 & 0 & 0 \\ 0 & 0 & \frac{1}{2}(\bar{C}_{11}^E - \bar{C}_{12}^E) & 0 & 0 \\ 0 & 0 & 0 & K^2 C_{55}^E & 0 \\ 0 & 0 & 0 & 0 & K^2 C_{55}^E \end{bmatrix} \begin{Bmatrix} \varepsilon_{xx} \\ \varepsilon_{yy} \\ \gamma_{xy} \\ \gamma_{xz} \\ \gamma_{yz} \end{Bmatrix} - \begin{bmatrix} 0 & 0 & \bar{e}_{31} \\ 0 & 0 & \bar{e}_{31} \\ 0 & 0 & 0 \\ -e_{15} & 0 & 0 \\ 0 & -e_{15} & 0 \end{bmatrix} \begin{Bmatrix} E_x \\ E_y \\ E_z \end{Bmatrix} \quad (4)$$

where the superscript (*p*) represents the variables in the piezoelectric material, $[\bar{C}]$ is the reduced stiffness matrix at constant electric field, $[\bar{e}]$ is the reduced matrix of piezoelectric electric constants and $\{E\}$ is the electric field. The components of reduced matrices are given in relation (A.1) of the Appendix.

3. Electric potential distribution in piezoelectric layer

For satisfying the Maxwell's equation and open and closed circuit electrical boundary conditions on the piezoelectric surfaces, it is needed to consider a combination of a parabolic and a linear function of thickness for transverse distribution of electric potential as follow (Wu *et al.* 2010)

$$\Phi(x, y, z) = \begin{cases} \left[1 - \left(\frac{z - h - h_p / 2}{h_p / 2} \right)^2 \right] \phi(x, y) + A(x, y)z + B(x, y) & h \leq z \leq h + h_p \\ \left[1 - \left(\frac{-z - h - h_p / 2}{h_p / 2} \right)^2 \right] \phi(x, y) + A'(x, y)z + B'(x, y) & -h - h_p \leq z \leq -h \end{cases} \quad (5)$$

where *A*, *B*, *A'* and *B'* are determined through satisfying the boundary conditions on the surfaces of piezoelectric layers.

The electric field is the negative of the gradient of electric potential (Wu *et al.* 2010), i.e.

$$\begin{Bmatrix} E_x \\ E_y \\ E_z \end{Bmatrix} = - \begin{Bmatrix} \frac{\partial \Phi}{\partial x} \\ \frac{\partial \Phi}{\partial y} \\ \frac{\partial \Phi}{\partial z} \end{Bmatrix} \quad (6)$$

The electric displacement is related to the strain field and electric field as (Wang *et al.* 2001)

$$\begin{Bmatrix} D_x \\ D_y \\ D_z \end{Bmatrix} = \begin{bmatrix} 0 & 0 & 0 & e_{15} & 0 \\ 0 & 0 & 0 & 0 & e_{15} \\ \bar{e}_{31} & \bar{e}_{31} & 0 & 0 & 0 \end{bmatrix} \begin{Bmatrix} \varepsilon_{xx} \\ \varepsilon_{yy} \\ \gamma_{xy} \\ \gamma_{xz} \\ \gamma_{yz} \end{Bmatrix} + \begin{bmatrix} \Xi_{11} & 0 & 0 \\ 0 & \Xi_{11} & 0 \\ 0 & 0 & \Xi_{33} \end{bmatrix} \begin{Bmatrix} E_x \\ E_y \\ E_z \end{Bmatrix} \quad (7)$$

When the outer surface of the plate is in contact with a medium with low permittivity such as air or vacuum and the inner surface is held at zero voltage (open circuit condition), the following surface boundary conditions are assumed

$$\begin{aligned} \Phi \Big|_{z=\pm h} &= 0 \\ D_z \Big|_{z=\pm(h+h_p)} &= 0 \end{aligned} \quad (8)$$

Also, when both surfaces are short circuited, the electrical boundary conditions for a closed circuit piezoelectric layer are represented as

$$\Phi \Big|_{z=\pm h} = \Phi \Big|_{z=\pm(h+h_p)} = 0 \quad (9)$$

Substituting Eqs. (5) and (7) into Eqs. (8) and (9) leads to the following electric potential distribution for open and closed circuit conditions, respectively

$$\Phi(x, y, z) = \begin{cases} \left[1 - \left(\frac{z - h - h_p / 2}{h_p / 2} \right)^2 \right] + \frac{4}{h_p} (z - h) \Big] \phi(x, y) + \frac{\bar{e}_{31}}{\Xi_{33}} (h + h_p) (\psi_{x,x} + \psi_{y,y}) (z - h) & h \leq z \leq h + h_p \\ \left[1 - \left(\frac{-z - h - h_p / 2}{h_p / 2} \right)^2 \right] - \frac{4}{h_p} (z + h) \Big] \phi(x, y) + \frac{\bar{e}_{31}}{\Xi_{33}} (h + h_p) (\psi_{x,x} + \psi_{y,y}) (-z - h) & -h - h_p \leq z \leq -h \end{cases} \quad (10a)$$

$$\Phi(x, y, z) = \begin{cases} \left[1 - \left(\frac{z - h - h_p / 2}{h_p / 2} \right)^2 \right] \phi(x, y) & h \leq z \leq h + h_p \\ \left[1 - \left(\frac{-z - h - h_p / 2}{h_p / 2} \right)^2 \right] \phi(x, y) & -h - h_p \leq z \leq -h \end{cases} \quad (10b)$$

Using the principle of minimum total potential energy, the equilibrium equations are obtained as

$$\begin{aligned} N_{xx,x} + N_{xy,y} &= 0 \\ N_{xy,x} + N_{yy,y} &= 0 \\ M_{xx,x} + M_{xy,y} - Q_{xz} &= 0 \\ M_{xy,x} + M_{yy,y} - Q_{yz} &= 0 \end{aligned} \quad (11)$$

$$N_{xx} w_{,xx} + 2N_{xy} w_{,xy} + N_{yy} w_{,yy} + Q_{xz,x} + Q_{yz,y} = 0$$

Where (N_{xx}, N_{xy}, N_{yy}) , (Q_{xz}, Q_{yz}) and (M_{xx}, M_{xy}, M_{yy}) are the force and moment resultants which obtained from relations (3) and (4) as

$$\begin{aligned} N_{xx} &= \int_{-h-h_p}^{h+h_p} \sigma_{xx} dz = F_1 u_{,x} + F_2 v_{,y} \\ N_{yy} &= \int_{-h-h_p}^{h+h_p} \sigma_{yy} dz = F_2 u_{,x} + F_1 v_{,y} \\ N_{xy} &= \int_{-h-h_p}^{h+h_p} \sigma_{xy} dz = \frac{1}{2} (F_1 - F_2) (u_{,y} + v_{,x}) \end{aligned} \quad (12a)$$

$$M_{xx} = \int_{-h-hp}^{h+hp} \sigma_{xx} z dz = Y_1 \psi_{x,x} + Y_3 \psi_{y,y} + \Theta_1 \phi$$

$$M_{yy} = \int_{-h-hp}^{h+hp} \sigma_{yy} z dz = Y_3 \psi_{x,x} + Y_1 \psi_{y,y} + \Theta_1 \phi \quad (12b)$$

$$M_{xy} = \int_{-h-hp}^{h+hp} \sigma_{xy} z dz = Y_2 (\psi_{x,y} + \psi_{y,x})$$

$$Q_{xz} = \int_{-h-hp}^{h+hp} \sigma_{xz} dz = C (\psi_x + w_{,x}) + \Theta_2 \phi_{,x} + \Theta_3 (\psi_{x,xx} + \psi_{y,xy})$$

$$Q_{yz} = \int_{-h-hp}^{h+hp} \sigma_{yz} dz = C (\psi_y + w_{,y}) + \Theta_2 \phi_{,y} + \Theta_3 (\psi_{x,xy} + \psi_{y,yy}) \quad (12c)$$

The constants in relations (12) have been introduced in the Appendix A as Eqs. (A.2 through A.4) and (A.6 through A.8) for closed and open circuit conditions, respectively.

Considering the adjacent equilibrium criterion these equations are represented as (Mohammadi *et al.* 2010)

$$N_{xx,x} + N_{xy,y} = 0$$

$$N_{xy,x} + N_{yy,y} = 0$$

$$M_{xx,x} + M_{xy,y} - Q_{xz} = 0$$

$$M_{xy,x} + M_{yy,y} - Q_{yz} = 0 \quad (13)$$

$$N_{xx}^0 w_{,xx} + 2N_{xy}^0 w_{,xy} + N_{yy}^0 w_{,yy} + Q_{xz,x} + Q_{yz,y} = 0$$

where $(N_{xx}^0, N_{xy}^0, N_{yy}^0)$ can be replaced by the pre-buckling forces obtained from equilibrium conditions.

Substituting relations (12a), (12b) and (12c) into Eq. (13) yield the force and moment resultants in terms of displacements as

$$F_1 u_{,xx} + \frac{1}{2}(F_1 - F_2) u_{,yy} + \frac{1}{2}(F_1 + F_2) v_{,xy} = 0$$

$$F_1 v_{,yy} + \frac{1}{2}(F_1 - F_2) v_{,xx} + \frac{1}{2}(F_1 + F_2) u_{,xy} = 0$$

$$(Y_1 - \Theta_3) \psi_{x,xx} + (Y_3 - \Theta_3) \psi_{y,xy} + (\Theta_1 - \Theta_2) \phi_{,x} + Y_2 (\psi_{x,yy} + \psi_{y,xy}) - C (\psi_x + w_{,x}) = 0 \quad (14)$$

$$(Y_1 - \Theta_3) \psi_{y,yy} + (Y_3 - \Theta_3) \psi_{x,xy} + (\Theta_1 - \Theta_2) \phi_{,y} + Y_2 (\psi_{x,xy} + \psi_{y,xx}) - C (\psi_y + w_{,y}) = 0$$

$$N_{xx}^0 w_{,xx} + 2N_{xy}^0 w_{,xy} + N_{yy}^0 w_{,yy} + C (\psi_{x,x} + \psi_{y,y} + w_{,xx} + w_{,yy}) + \Theta_2 (\phi_{,xx} + \phi_{,yy}) + \Theta_3 (\psi_{x,xxx} + \psi_{y,xyy} + \psi_{x,xyy} + \psi_{y,yyy}) = 0$$

It should be noted that, for symmetric laminated plates, the first two equations are decoupled from last three equations and may be neglected (Jomehzadeh and Saidi 2009).

It can be seen that, the following relation exists between the constants

$$Y_3 = Y_1 - 2Y_2 \quad (15)$$

Using relation (15), the last three Eq. (14) can be rewritten as

$$(Y_1 - \Theta_3) (\psi_{x,xx} + \psi_{y,xy}) + (\Theta_1 - \Theta_2) \phi_{,x} + Y_2 (\psi_{x,yy} - \psi_{y,xy}) - C (\psi_x + w_{,x}) = 0$$

$$(Y_1 - \Theta_3) (\psi_{x,xy} + \psi_{y,yy}) + (\Theta_1 - \Theta_2) \phi_{,y} - Y_2 (\psi_{x,xy} - \psi_{y,xx}) - C (\psi_y + w_{,y}) = 0$$

$$N_{xx}^0 w_{,xx} + 2N_{xy}^0 w_{,xy} + N_{yy}^0 w_{,yy} + C (\psi_{x,x} + \psi_{y,y} + w_{,xx} + w_{,yy}) + \Theta_2 (\phi_{,xx} + \phi_{,yy}) + \Theta_3 (\psi_{x,xxx} + \psi_{y,xyy} + \psi_{x,xyy} + \psi_{y,yyy}) = 0 \quad (16)$$

Besides Eq. (12), the variables should also satisfy the Maxwell's equation (Askari Farsangi and Saidi 2012, Askari Farsangi *et al.* 2013), namely

$$\int_h^{h+hp} \left(\frac{\partial D_x}{\partial x} + \frac{\partial D_y}{\partial y} + \frac{\partial D_z}{\partial z} \right) dz + \int_{-h-hp}^{-h} \left(\frac{\partial D_x}{\partial x} + \frac{\partial D_y}{\partial y} + \frac{\partial D_z}{\partial z} \right) dz = 0 \quad (17)$$

Referring to relations (10a) and (10b), it is seen that the electrical potential function is related to the displacement field components in both open and closed circuit cases. By considering the in-plane displacement components on middle plane (u,v) the magnitudes of the electric displacements in upper and bottom piezoelectric layers are different. Hence, the Maxwell's equation is not identical for both piezoelectric layers. So, the integration should be done on both upper and lower piezoelectric layers (Rahmat Talabi and Saidi 2013).

Utilizing Eqs. (10a) and (10b) into Eq. (17), the Maxwell's equation is obtained free of u and v components as

$$\eta_1 (\psi_{x,x} + \psi_{y,y}) + \eta_2 (w_{,xx} + w_{,yy}) + \eta_3 (\psi_{x,xxx} + \psi_{y,xyy} + \psi_{x,xyy} + \psi_{y,yyy}) + \eta_4 \phi + \eta_5 (\phi_{,xx} + \phi_{,yy}) = 0 \quad (18)$$

where $\eta_i (i=1$ to 5) are given in the Appendix A as equations (A.5) and (A.9) for closed and open circuit conditions, respectively.

Eqs. (16) and (18) are four coupled equations in terms of w, ψ_x, ψ_y and ϕ . These equations can be decoupled with the help of the following auxiliary functions (Mohammadi *et al.* 2010, Saidi and Jomehzadeh 2009)

$$\phi_1 = \psi_{x,x} + \psi_{y,y}$$

$$\phi_2 = \psi_{x,y} - \psi_{y,x} \quad (19)$$

Using relations (19), the governing equations can be written as

$$(Y_1 - \Theta_3) \phi_{1,x} + (\Theta_1 - \Theta_2) \phi_{1,x} + Y_2 \phi_{2,y} - C (\psi_x + w_{,x}) = 0 \quad (20a)$$

$$(Y_1 - \Theta_3) \phi_{1,y} + (\Theta_1 - \Theta_2) \phi_{1,y} - Y_2 \phi_{2,x} - C (\psi_y + w_{,y}) = 0 \quad (20b)$$

$$N_{xx}^0 w_{,xx} + 2N_{xy}^0 w_{,xy} + N_{yy}^0 w_{,yy} + C (\phi_1 + \nabla^2 w) + \Theta_2 (\nabla^2 \phi) + \Theta_3 (\nabla^2 \phi_1) = 0 \quad (20c)$$

$$\eta_1 \phi_1 + \eta_2 \nabla^2 w + \eta_3 \nabla^2 \phi_1 + \eta_4 \phi + \eta_5 \nabla^2 \phi = 0 \quad (20d)$$

where ∇^2 is the two dimensional Laplace operator in Cartesian coordinate.

Differentiation of Eq. (20a) with respect to x and Eq. (20b) with respect to y and adding the results yields

$$(\Upsilon_1 - \Theta_3)\nabla^2\varphi_1 + (\Theta_1 - \Theta_2)\nabla^2\phi - C(\varphi_1 + \nabla^2w) = 0 \quad (21)$$

Eqs. (20c), (20d) and Eq. (21) are in terms of φ_1 , φ and w . Eliminating of φ_1 and φ from these equations yields (Mohammadi *et al.* 2010)

$$\begin{aligned} & m_1\nabla^6w + m_2\nabla^4w + m_3\nabla^2w \\ & m_4\nabla^4\left(N_{xx}^0w_{,xx} + 2N_{xy}^0w_{,xy} + N_{yy}^0w_{,yy}\right) + \\ & m_5\nabla^2\left(N_{xx}^0w_{,xx} + 2N_{xy}^0w_{,xy} + N_{yy}^0w_{,yy}\right) + \\ & m_6\left(N_{xx}^0w_{,xx} + 2N_{xy}^0w_{,xy} + N_{yy}^0w_{,yy}\right) = 0 \end{aligned} \quad (22)$$

The constants m_i ($i=1..6$) are defined in the Appendix B. Also, φ_1 and φ can be easily obtained in terms of w . Similarly, differentiation of Eq. (20a) with respect to y and Eq. (20b) with respect to x and subtracting the results, it is concluded that

$$\Upsilon_2\nabla^2\varphi_2 - C\varphi_2 = 0 \quad (23)$$

Which can be solved for finding φ_2 .

4. Electrical and mechanical boundary conditions

It is assumed that the plate is simply supported at two opposite edges in y -direction ($x=0, x=a$) and it has arbitrary boundary conditions at two other edges (e.g., Clamped, Simply supported and Free). Using the principle of minimum total potential energy, the mechanical boundary conditions are obtained as follow:

Clamped:

$$w = \psi_x = \psi_y = 0 \quad (24a)$$

Simply supported:

$$w = \psi_x = M_{yy} = 0 \quad (24b)$$

Free:

$$Q_y + N_{xy}^0w_{,x} + N_{yy}^0w_{,y} = M_{yy} = M_{xy} = 0 \quad (24c)$$

Furthermore, the plate is assumed to be insulated at the edges in y -direction. So the electrical flux conservation equation leads to the following electrical boundary conditions (Farsangi and Saidi 2012, Farsangi *et al.* 2013)

$$\int_h^{h+h_p} D_y(x, y, z) dz + \int_{-h}^{-h-h_p} D_y(x, y, z) dz = 0 \quad (25)$$

Through the text, the letters S, C and F indicate that the edge is simply supported, clamped and free respectively.

5. Buckling analysis

In this study, a rectangular plate with length a and

width b which is subjected to in-plane loads is considered. The pre-buckling forces are obtained through using the equilibrium conditions

$$\begin{aligned} N_{xx}^0 &= \varsigma_1 P_1 \\ N_{yy}^0 &= \varsigma_2 P_1 \\ N_{xy}^0 &= 0 \end{aligned} \quad (26)$$

where P_1 is the force per unit length, ς_1 and ς_2 are the load parameter which indicate the loading conditions in x - and y -directions, respectively. If the the load ratio is showed by $R=\varsigma_2/\varsigma_1$ then, $R=0$ indicates a plate subjected to uniaxial loading in x - direction, $R=1$ shows a plate with biaxial compressive loading in the x - and y - directions, and $R=-1$ represents a plate under compressive and tensile loading in the x - and y -directions, respectively.

Since the plate is simply supported along two opposite edges in the y -directions, and in order to reduce the governing partial differential equations to a system of ordinary ones, the functions w and φ_2 can be expressed as (Bodaghi and Saidi 2011b)

$$\begin{aligned} w &= \sum_{m=1}^{\infty} f(y) \sin\left(\frac{m\pi x}{a}\right) \\ \varphi_2 &= \sum_{m=1}^{\infty} g(y) \cos\left(\frac{m\pi x}{a}\right) \end{aligned} \quad (27)$$

Substituting (27) into (22) and (23), respectively, the following two ordinary differential equations are obtained

$$\begin{aligned} & (m_1 + m_4 N_{yy}^0) \frac{d^6}{dy^6} f(y) + (-3m_1\beta^2 + m_2 + m_5 N_{yy}^0 - 2m_4 N_{yy}^0 \beta^2 \\ & - m_4 N_{xx}^0 \beta^2) \frac{d^4}{dy^4} f(y) + (3m_1\beta^4 - 2m_2\beta^2 + m_3 + m_4 N_{yy}^0 \beta^4 \\ & + 2m_4 N_{xx}^0 \beta^4 + m_6 N_{yy}^0 - m_5 N_{yy}^0 \beta^2 - m_5 N_{xx}^0 \beta^2) \frac{d^2}{dy^2} f(y) \\ & + (m_5 N_{xx}^0 \beta^4 - m_4 N_{xx}^0 \beta^6 - m_6 N_{xx}^0 \beta^2 - m_1\beta^6 + m_2\beta^4 - m_3\beta^2) f(y) = 0 \end{aligned} \quad (28a)$$

$$\Upsilon_2 \frac{d^2}{dy^2} g(y) - (C + \Upsilon_2 \beta^2) g(y) = 0 \quad (28b)$$

where $\beta=m\pi x/a$. The general solutions of Eqs. (28a) and (28b) can be expressed as

$$f(y) = C_1 \sinh(\lambda_1 y) + C_2 \cosh(\lambda_1 y) + C_3 \sinh(\lambda_2 y) + C_4 \cosh(\lambda_2 y) + C_5 \sinh(\lambda_3 y) + C_6 \cosh(\lambda_3 y) \quad (29a)$$

$$g(y) = C_7 \sinh(\lambda_4 y) + C_8 \cosh(\lambda_4 y) \quad (29b)$$

where, C_i ($i = 1, \dots, 8$) are eight unknown constants. The variables λ_i ($i = 1, 2, 3$) are given by Bodaghi and Saidi (2010) and λ_4 is given in the Appendix as Eq. (B.1). It should be noted that, the general solutions (29a) are valid for real values of λ_i . For imaginary ones \sinh and \cosh should be replaced by \sin and \cos , respectively. By imposing the mechanical and electrical boundary conditions

Table 1 Comparison of the non-dimensional buckling loads for isotropic core plate with (Mohammadi *et al.* 2010) for different boundary conditions

R	2h/a	a/b	Boundary condition					
			SFSF	SFSS	SFSC	SCSS	SCSC	SSSS
0	0.5	Reference	9.315383	10.396280	10.629458	16.222707	18.021045	14.896187
		Open	9.315587	10.396489	10.629663	16.223111	18.021476	14.896569
		Closed	9.315373	10.396110	10.629436	16.222110	18.020975	14.896148
		Reference	8.599118	9.551170	9.727484	14.494771	15.750964	13.515629
		Open	8.599174	9.551226	9.727537	14.494873	15.751055	13.515737
		Closed	8.599085	9.550110	9.727444	14.494110	15.750110	13.515564
	1	Reference	9.101957	13.238391	15.365298	51.550649	63.003858*	37.370789
		Open	9.102116	13.238572	15.365461	51.551661	63.004577*	37.371667
		Closed	9.101942	13.238362	15.365252	51.550110	63.003041*	37.370632
		Reference	8.401412	11.998489	13.548684	40.968426	42.873560*	32.211740
		Open	8.401453	11.998518	13.548686	40.968430	42.873222*	32.211890
		Closed	8.401382	11.998436	13.548610	40.967993	42.872110*	32.211506
1	0.5	Reference	9.041739	9.371949	9.439394	12.727113	13.944616	11.916950
		Open	9.048915	9.372059	9.439493	12.727433	13.944955	11.917255
		Closed	9.048767	9.371931	9.439375	12.726110	13.944566	11.916918
		Reference	8.288779	8.518930	8.558778	11.423114	12.299795	10.812503
		Open	8.288800	8.518938	8.558781	11.423198	12.299872	10.812590
		Closed	8.288747	8.518895	8.558742	11.420110	12.299720	10.812451
	1	Reference	8.860416	9.824325	10.502725	24.192699	33.320627	18.685395
		Open	8.860528	9.824380	10.502749	24.193201	33.321179	18.685834
		Closed	8.860402	9.820110	10.502697	24.191110	33.320320	18.685316
		Reference	8.140908	8.806588	9.267746	19.646211	24.857923	16.105870
		Open	8.140925	8.806571	9.267714	19.646235	24.857839	16.105945
		Closed	8.140879	8.808890	9.267700	19.646019	24.857598	16.105753
-1	0.5	Reference	9.391407	11.226550	11.576414	22.124398	25.010505	19.861583
		Open	9.391601	11.226800	11.576665	22.124940	25.011079	19.862091
		Closed	9.391369	11.226527	11.576388	22.124110	25.010391	19.861530
		Reference	8.671561	10.316867	10.576026	19.600831	21.486708	18.020839
		Open	8.671625	10.316938	10.576095	19.600960	21.486813	18.020983
		Closed	8.671528	10.316825	10.575981	19.600110	21.486556	18.020752
	1	Reference	9.208877	18.390228	22.947335	78.403323*	85.946832*	72.083357*
		Open	9.209057	18.390563	22.947697	78.404352*	85.947670*	72.084500*
		Closed	9.208860	18.390110	22.947238	78.402110*	85.945615*	72.082652*
		Reference	8.500262	16.645443	19.726678	54.936510*	57.484447*	52.588166*
		Open	8.500312	16.645514	19.726708	54.936150*	57.483967*	52.587908*
		Closed	8.500231	16.645110	19.726545	54.935663*	57.483488*	52.587416*

on the edges of plate, a set of homogenous algebraic equations are obtained. The buckling load can be determined by setting the determinant of coefficient matrix to zero.

6. Validation of results

In order to verify the accuracy of the present

formulations, the critical buckling loads obtained from the present method are compared with those available in the literature for isotopic plates under in-plane loads (Mohammadi *et al.* 2010). In Table 1, comparison of the non-dimensional critical buckling loads for isotropic plates with Levy boundary conditions under different loading conditions is made between the results obtained by the present solution and those reported by Mohammadi *et al.* (2010). In order to obtain solutions for a single layer

Table 2 Material properties of some common piezoelectric materials

materials	Elastic constants (GPa)					Electric constants (C/m ²)			Dielectric constants (C/Vm)	
	C_{11}^E	C_{33}^E	C_{55}^E	C_{12}^E	C_{13}^E	e_{33}	$-e_{31}$	e_{15}	Ξ_{11}	Ξ_{33}
PZT-4	132	115	26	71	73	14.1	4.1	10.5	7.124e-9	5.841 e-9
PZT-5A	121	111	21.1	75.9	75.4	15.8	5.4	12.3	8.11 e-9	7.35 e-9
PZT-6B	168	163	35.5	84.7	84.2	7.10	0.9	4.60	3.60 e-9	3.42 e-9
PZT-7A	148	131	25.3	76.1	81.3	9.50	2.1	9.20	4.07 e-9	2.08 e-9
PZT-8	137	123	31.3	69.9	71.1	17.5	4.0	10.4	7.97 e-9	5.14 e-9

Table 3 The critical buckling load of a plate with constant total thickness ($a/b=1, H=0.1$)

R	h/h_p	Boundary conditions						
		SCSC	SCSS	SSSS	SFSC	SFSS	SFSF	
1	Null	1	219.050	162.590	127.452	72.585	68.119	61.669
		0.5	225.608	166.396	129.873	73.953	69.309	62.613
	Closed	1	233.219	170.124	131.828	74.491	69.699	62.893
		0.5	237.046	173.085	134.243	75.381	70.617	63.847
	Open	1	258.703	194.332	153.746	75.759	72.052	67.599
		0.5	270.647	202.007	159.204	77.465	73.660	69.144
0	Null	1	475.410	344.461	254.904	105.860	91.773	63.293
		0.5	491.147	353.108	259.747	107.800	93.260	64.227
	Closed	1	509.759	361.883	263.657	108.819	93.871	64.565
		0.5	517.129	367.917	268.478	110.398	95.329	65.644
	Open	1	554.608	409.538	307.527	116.550	102.483	72.095
		0.5	579.888	425.954	318.479	119.643	105.121	73.952
-1	Null	1	546.515 ⁽²⁾	506.446 ⁽²⁾	471.749 ⁽²⁾	156.660	127.234	63.985
		0.5	568.020 ⁽²⁾	524.178 ⁽²⁾	486.543 ⁽²⁾	159.780	129.271	64.920
	Closed	1	595.455 ⁽²⁾	545.968 ⁽²⁾	504.036 ⁽²⁾	161.991	130.278	65.296
		0.5	602.818 ⁽²⁾	553.860 ⁽²⁾	512.173 ⁽²⁾	164.523	132.479	66.430
	Open	1	629.635	590.571	555.834	179.271	146.931	74.110
		0.5	661.186	619.434	582.363	184.876	151.161	76.135

isotropic plate, the thickness of the piezoelectric layers set to zero. It can be concluded from Table 1 that the results are in good correlation with the those reported by Mohammadi *et al.* (2010).

7. Numerical results and discussion

After verification of the results, the numerical results for buckling of a transversely isotropic plate with two surface bounded piezoelectric layers are presented. The numerical values for the Young's modulus, Poisson's ratio and the shear modulus of the core plate are considered to be $E=70$ (GPa), $\nu=0.3$ and $G_\xi=0.15E$, respectively (Bodaghi and Saidi 2011a). Moreover, the piezoelectric layer is made of *PZT-4* whose material properties are listed in Table 2.

Here, two set of numerical results have been presented. In the first set of numerical results, it is assumed that the plate has a constant overall thickness of $H=2h+2h_p=0.1$ and h_p varies from 0 to 0.05, that means $h_p=0$ and $h_p=0.05$ are related to the plate made of pure transversely isotropic

and pure piezoelectric materials, respectively. Fig. 2 depicts the variation of critical buckling load (in Mega Newton per meter (MN/m)) versus piezoelectric thickness for a SCSC plate subjected to the biaxial compression under open, closed and null surface conditions which null means that the electrical effect of piezoelectric layer is removed by setting the electrical coefficient of piezoelectric material (e_{ij}) to zero to taken into account the mechanical effect only. This figure shows that for all electrical conditions, the highest and lowest values of the critical buckling loads are corresponded to pure *PZT-4* plate and pure transversely isotropic plate, respectively. Furthermore, it is seen that the critical buckling loads obtained from open circuit condition are significantly higher than those of closed circuit and null. It can be concluded that the effective stiffness of the smart laminated plate with open circuit surface condition is larger than that of the closed circuit one. Such a phenomenon can be attributed to the different electric potential distributions along thickness direction of piezoelectric laminated plate for open and closed circuit conditions.

In Tables 3 and 4, in constant overall thickness and all

Table 4 The critical buckling load of a plate with constant total thickness ($a/b=0.5, H=0.1$)

R	h/h_p	Boundary conditions						
		SCSC	SCSS	SSSS	SFSC	SFSS	SFSF	
1	Null	1	95.584	87.608	82.242	65.530	65.078	62.885
		0.5	97.255	89.030	83.514	66.600	66.124	63.853
	Closed	1	98.515	89.995	84.315	66.985	66.506	64.195
		0.5	100.364	91.695	85.935	67.950	67.488	65.206
	Open	1	115.838	106.444	100.087	70.798	70.629	69.339
		0.5	119.885	110.028	103.386	72.416	72.252	70.965
0	Null	1	123.237	111.544	102.803	73.695	72.128	64.680
		0.5	125.477	113.392	104.392	74.819	73.205	65.621
	Closed	1	127.219	114.661	105.394	75.337	73.680	66.030
		0.5	129.585	116.841	107.418	76.633	74.969	67.208
	Open	1	149.017	135.387	125.105	85.231	83.808	75.611
		0.5	154.254	139.974	129.229	87.592	86.141	77.728
-1	Null	1	170.199	151.773	137.070	80.147	77.828	65.169
		0.5	173.532	154.388	139.189	81.368	78.979	66.111
	Closed	1	176.297	156.283	140.518	81.996	79.537	66.548
		0.5	179.443	159.197	143.224	83.467	80.985	67.769
	Open	1	204.882	183.838	166.812	94.611	92.145	77.289
		0.5	212.148	190.110	172.310	97.427	94.867	79.556

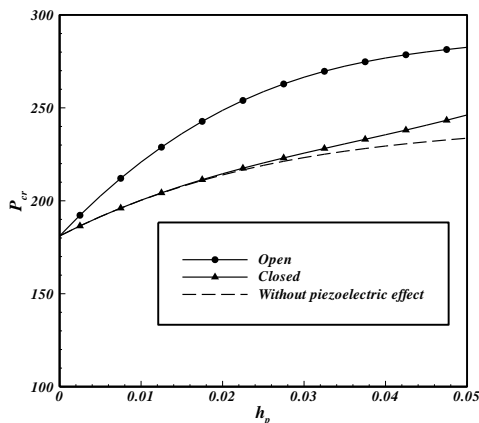


Fig. 2 The critical buckling load of SCSC plate with constant overall thickness versus h_p ($a/b=1, R=1$)

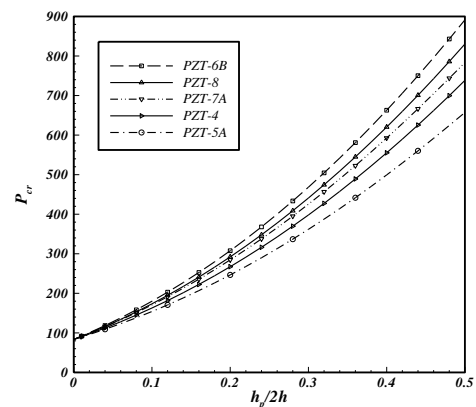


Fig. 4 The critical buckling load for a SCSC plate made of various piezoelectric materials versus $h_p/2h$ for open circuit condition ($a/b=0.5, R=1, 2h/a=0.1$)

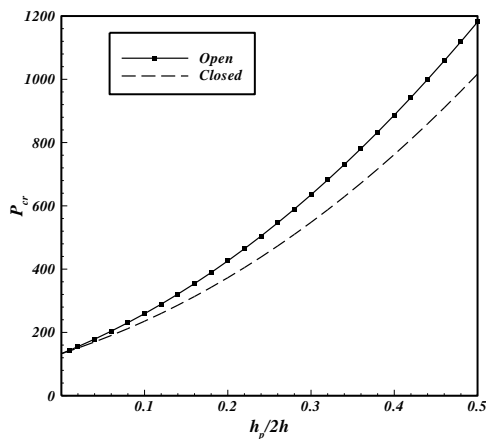


Fig. 3 The critical buckling load of SCSS plate versus $h_p/2h$ ($2h/a=0.1, a/b=0.5, R=-1$)

mechanical boundary conditions, the critical buckling load of plates in null, open and closed electrical conditions is tabulated for $a/b=1$ and 0.5 , respectively. From these tables it can be concluded that the critical buckling load for null condition is less than that of closed and open circuit conditions, as predicted.

In the following of the numerical results, it is assumed that the thickness of host layer to be constant ($2h=0.1$). In Fig. 3, the critical buckling load of a SCSS plate under biaxial compression and tension are compared in open and closed circuit conditions. It is observed that in a special h_p , the critical buckling load for closed circuit piezoelectric layer is less than open one. Moreover, for both open and closed circuit conditions, the critical buckling load increases with the increase of piezoelectric layer thickness.

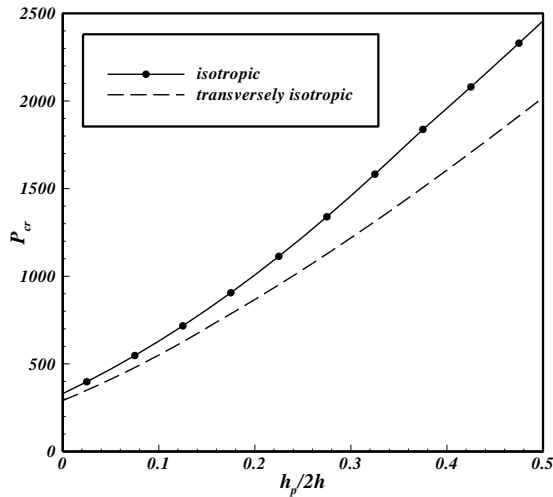
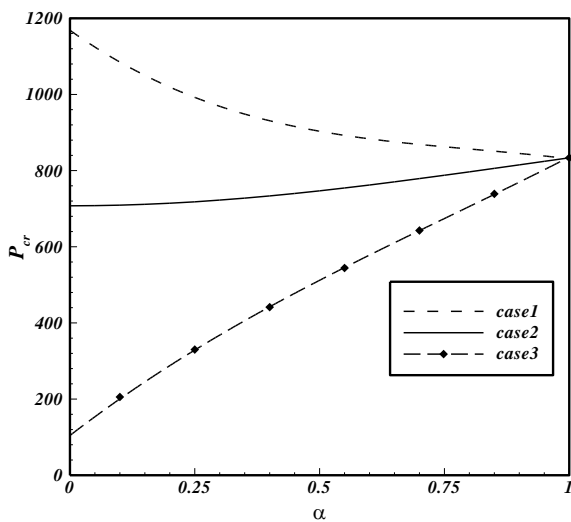
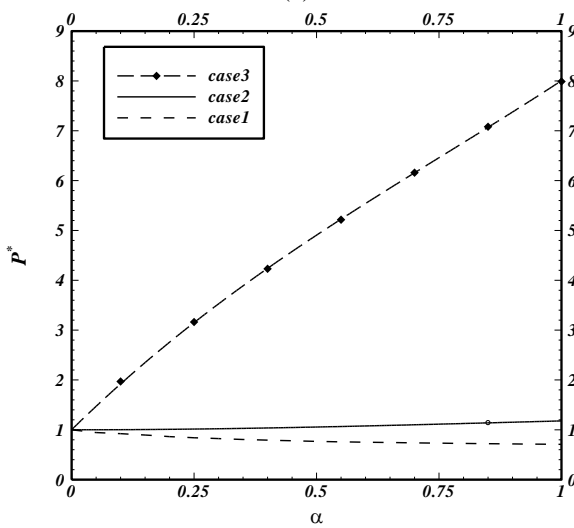


Fig. 5 The critical buckling load of SCSS plate versus $h_p/2h$ for open circuit condition ($a/b=1, 2h/a=0.1, R=0$)

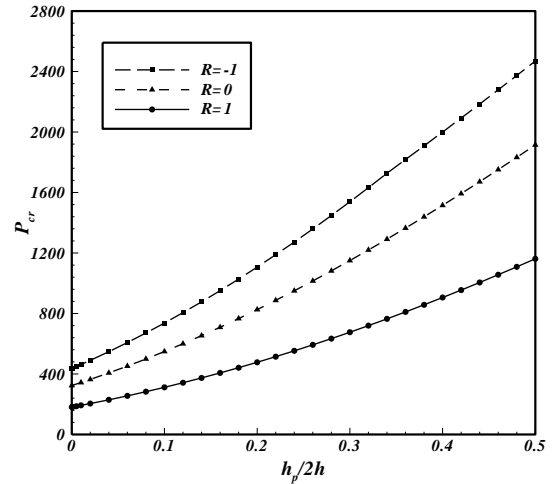


(a)

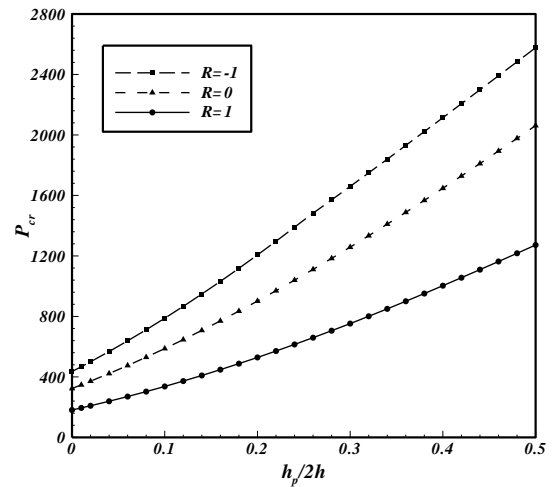


(b)

Fig. 6 (a) The non-dimensional critical buckling load and (b) The critical buckling load for SSSS plate versus α for open circuit condition ($a/b=0.5, 2h/a=0.1, R=0$)



(a) Closed circuit condition



(b) open circuit condition

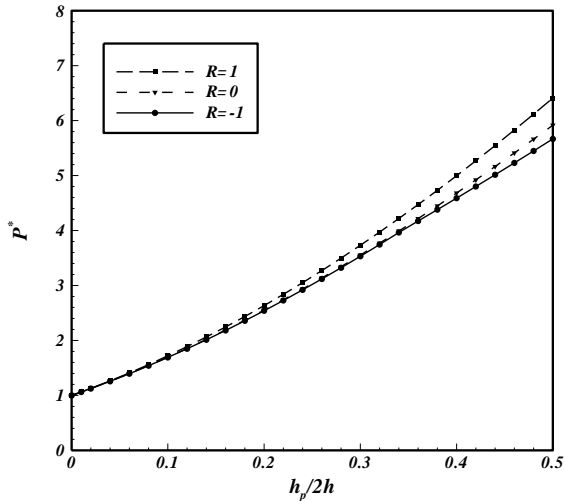
Fig. 7 The critical buckling load of SCSS plate versus $h_p/2h$ ($2h/a=0.1, a/b=1$)

For five different piezoelectric materials, the critical buckling load versus $h_p/2h$ is plotted in figure 4. This figure shows that the least and the most value of the critical buckling loads are related to *PZT-5A* and *PZT-6B* layers, respectively. Focusing on properties of *PZT-5A* and *PZT-6B* in table 2, it can be seen that *PZT-6B* has the least values of dielectric and electric constants and the highest values of reduced stiffness matrix components and this is completely reverse for *PZT-5A*.

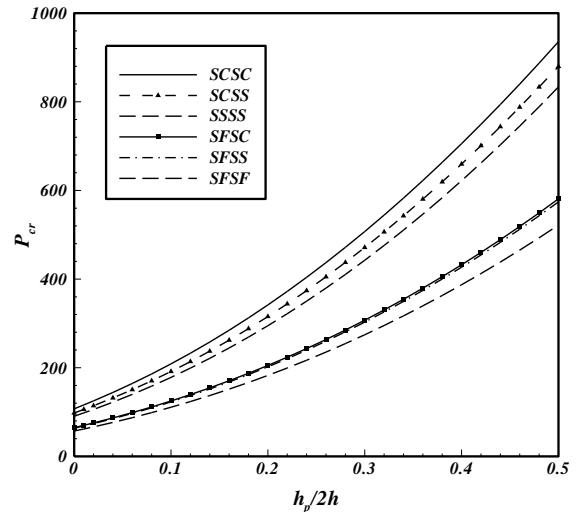
A comparison between the critical buckling load of a transversely isotropic plate and an isotropic plate both with two surface bounded piezoelectric layers is performed in Fig. 5. It can be seen that, in all values of h_p , the the critical buckling load of isotropic plate is more than that of transeversely isotropic one, as predicted.

In order to study of piezoelectric effect, the relative critical buckling load P^* is defined as

$$P^* = \frac{P_{cr} \Big|_{with\ piezoelectric\ layer}}{P_{cr} \Big|_{without\ piezoelectric\ layer}} \quad (30)$$

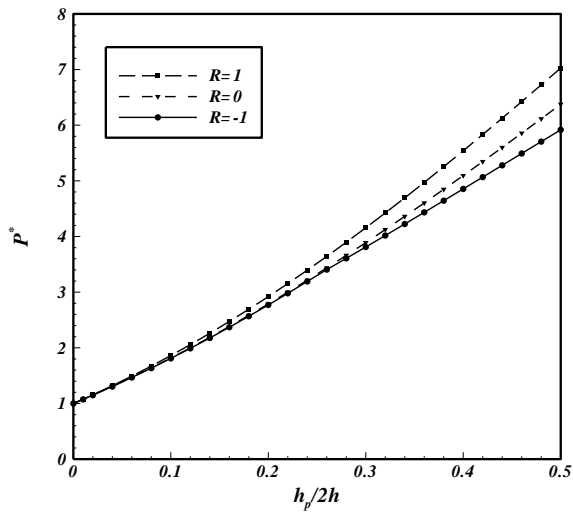


(a) Closed circuit condition



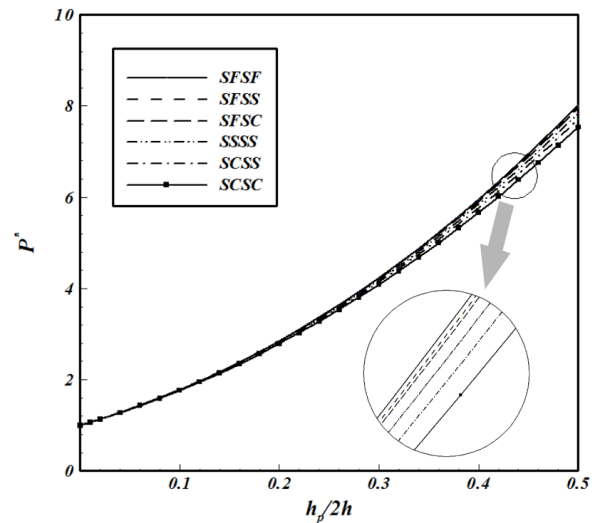
(b) open circuit condition

Fig. 9 Continued

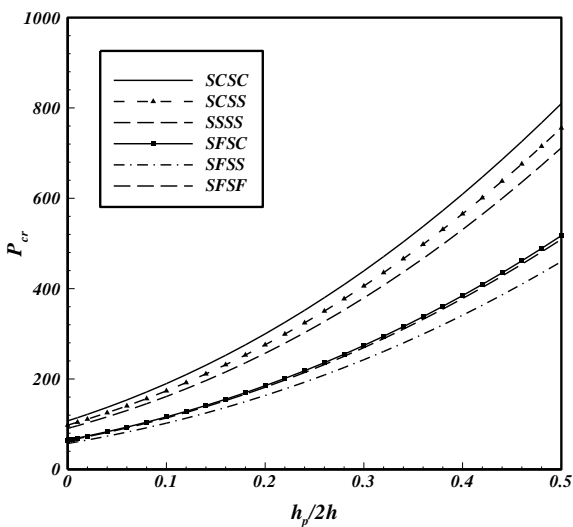


(b) open circuit condition

Fig. 8 The non-dimensional critical buckling load of SCSC plate versus $h_p/2h$ ($2h/a=0.1$, $a/b=1$)

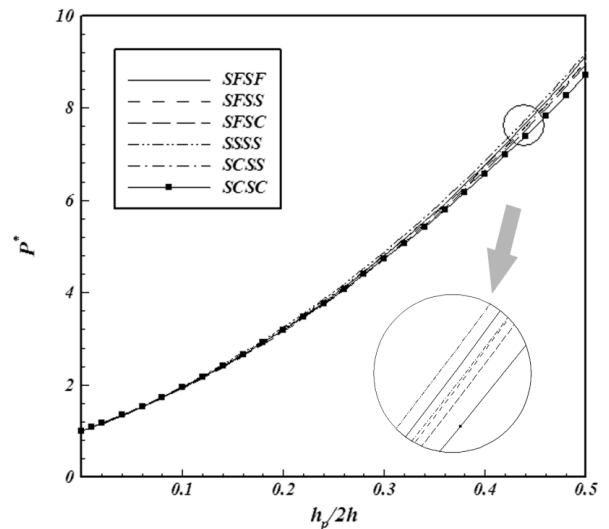


(a) Closed circuit condition



(a) Closed circuit condition

Fig. 9 The critical buckling load for all Levy boundary conditions versus $h_p/2h$ ($2h/a=0.1$, $a/b=0.5$, $R=0$)



(b) open circuit condition

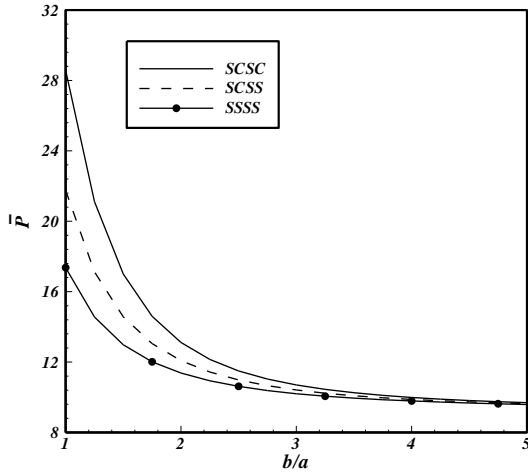
Fig. 10 The non-dimensional critical buckling load for all Levy boundary conditions versus $h_p/2h$ ($2h/a=0.1$, $a/b=0.5$, $R=0$)

Table 5 The critical buckling load of plate under different boundary and loading conditions for open and closed circuit ($a/b=1, h_p/2h=0.2$)

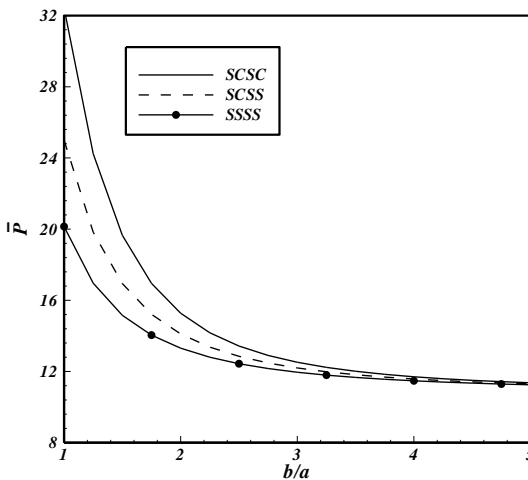
R	2h/a	Boundary condition						
		SCSC	SCSS	SSSS	SFSC	SFSS	SFSF	
1	Closed	0.1	477.286	375.422	306.811	177.439	168.230	155.249
		0.08	276.678	210.428	167.815	95.819	90.382	82.497
		0.05	79.141	57.343	44.228	25.029	23.381	21.040
	Open	0.1	528.713	421.742	348.431	182.254	174.505	165.251
		0.08	311.037	239.320	192.479	98.830	94.142	88.315
		0.05	90.935	66.305	51.364	25.984	24.552	22.711
0	Closed	0.1	825.752 ⁽²⁾	783.130	613.675	258.832	228.844	159.946
		0.08	495.592 ⁽²⁾	442.799	335.639	139.937	122.333	84.853
		0.05	149.950 ⁽²⁾	122.236	88.470	36.520	31.427	21.580
	Open	0.1	901.668 ⁽²⁾	867.262 ⁽²⁾	696.954	276.412	247.028	175.390
		0.08	549.965 ⁽²⁾	501.787	384.975	150.220	132.731	93.502
		0.05	170.870 ⁽²⁾	141.071	102.728	39.500	34.343	23.936
-1	Closed	0.1	1106.773 ⁽²⁾	1056.990 ⁽²⁾	1011.143 ⁽²⁾	376.432	317.070	161.731
		0.08	667.203 ⁽²⁾	627.600 ⁽²⁾	592.212 ⁽²⁾	205.696	169.669	85.812
		0.05	204.591 ⁽²⁾	186.439 ⁽²⁾	171.260 ⁽²⁾	54.452	43.597	21.820
	Open	0.1	1206.373 ⁽²⁾	1159.658 ⁽²⁾	1116.077 ⁽²⁾	411.976	350.110	179.403
		0.08	738.555 ⁽²⁾	699.508 ⁽²⁾	664.130 ⁽²⁾	227.036	188.597	95.699
		0.05	232.421 ⁽²⁾	213.024 ⁽²⁾	196.602 ⁽²⁾	60.830	48.869	24.499

Table 6 The critical buckling load of plate under different boundary and loading conditions for open and closed circuit ($a/b=0.5, h_p/2h=0.2$)

R	2h/a	Boundary condition						
		SCSC	SCSS	SSSS	SFSC	SFSS	SFSF	
1	Closed	0.1	234.145	217.246	205.440	163.420	162.606	158.034
		0.08	126.699	116.695	109.888	87.313	86.792	84.090
		0.05	33.002	30.105	28.177	22.431	22.266	21.475
	Open	0.1	267.351	248.867	235.917	171.788	171.433	168.600
		0.08	145.839	134.669	127.009	92.403	92.165	90.396
		0.05	38.373	35.052	32.837	23.981	23.897	23.340
0	Closed	0.1	299.889	275.703	256.870	185.156	181.734	163.539
		0.08	162.898	148.392	137.369	98.596	96.611	86.768
		0.05	42.656	38.380	35.230	25.190	24.630	22.062
	Open	0.1	341.739	315.517	294.900	205.191	202.086	182.721
		0.08	187.210	171.101	158.762	109.851	108.022	97.460
		0.05	49.560	44.667	41.047	28.264	27.733	24.950
-1	Closed	0.1	409.181	372.876	342.512	201.170	196.179	164.836
		0.08	223.727	201.369	183.164	107.218	104.297	87.455
		0.05	59.216	52.353	46.977	27.413	26.578	22.231
	Open	0.1	464.841	426.048	393.204	226.081	220.991	186.018
		0.08	256.410	231.871	211.683	121.214	118.176	99.240
		0.05	68.689	60.879	54.729	31.222	30.331	25.398



(a) Closed circuit condition



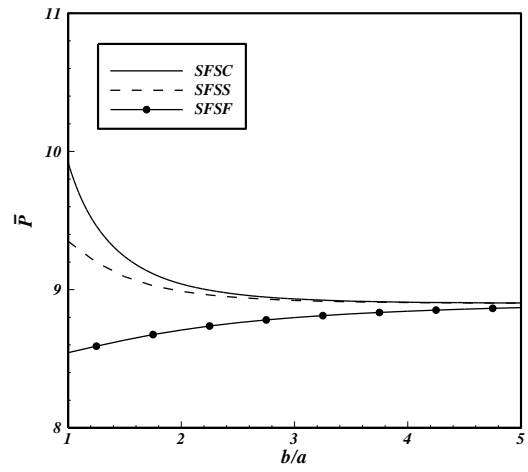
(b) open circuit condition

Fig. 11 The non-dimensional critical buckling load for SCSC, SCSS and SSSS plate versus b/a ($2h/a=0.1, R=1$)

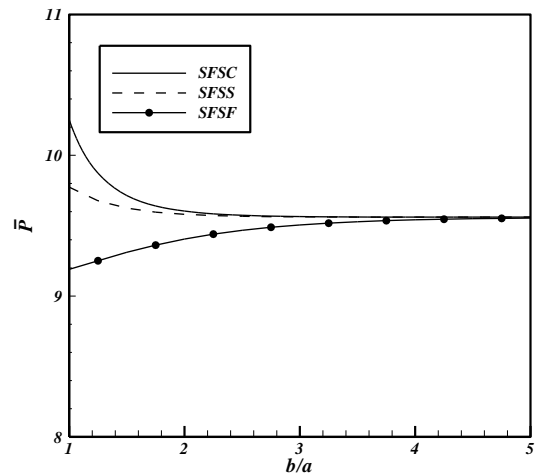
The critical buckling load without piezoelectric layer is obtained by setting the piezoelectric layer thickness equal to zero.

In order to study the effects of piezoelectric matrix constants on the buckling load, the variation of both the critical buckling load P_{cr} and the relative critical buckling load P^* versus the parameter α are plotted in Fig. 6. The parameter α which varies between 0 to 1 is a multiplier of matrix of piezoelectric constants. $\alpha=1$ means the matrix of piezoelectric constants is belonged to *PZT-4* and $\alpha=0$ means the matrix of piezoelectric constants is equal to zero. Cases 1 through 3 are related to variation in the reduced matrix of dielectric constants $[\Xi]$, the reduced matrix of piezoelectric electric constants $[\bar{e}]$ and the reduced stiffness matrix $[\bar{C}]$, respectively. From these figures, it can be found that in cases 2 and 3 unlike the case 1 the critical buckling load and the non-dimensional critical buckling load increase as α increases. Also, these figures show that the effect of variation in reduced stiffness matrix $[\bar{C}]$ on the critical buckling load is more considerable.

For a SCSC square plate in both open and closed circuit conditions, the variation of the critical buckling load (P_{cr})



(a) Closed circuit condition



(b) open circuit condition

Fig. 12 The non-dimensional critical buckling load for SFSC, SFSS and SFSC plate versus b/a ($2h/a=0.1, R=1$)

and relative critical buckling load (P^*) versus the piezoelectric layer thickness to the core thickness ratio are depicted in Figs. 7 and 8, respectively. Comparing Figs. 7 and 8, it can be found that the ascending order of loading conditions for the critical buckling load P_{cr} and the relative critical buckling load P^* is completely reverse.

In Figs. 9 and 10 for both open and closed circuit conditions, the critical buckling load P_{cr} and the relative critical buckling load P^* are plotted, respectively, for 6 different mechanical boundary conditions. In the case of the critical buckling load P_{cr} , it can be concluded that for both closed and open circuit conditions, stronger constraints on boundary conditions lead to higher critical buckling loads which means, the mechanical boundary conditions can be sorted in ascending order of critical buckling load as SFSC, SFSS, SFSC, SSSS, SCSS and SCSC.

Moreover, the ascending order of P^* for closed circuit condition is different that of P_{cr} . The open circuit condition has no special ascending order of P^* at all values of h_p , that means, at each special h_p , there is a special ascending order of P^* .

Now, the non-dimensional critical buckling load \bar{P} is defined as

Table 7 The critical buckling load and mode number of square plate for open and closed circuit ($R=-1$, $2h/a=0.1$)

Bc's	SSSS		SCSC		SCSS		
	$h_p/2h$	Closed	Open	closed	open	closed	Open
0		387.471 ⁽²⁾	387.471 ⁽²⁾	435.755 ⁽²⁾	435.755 ⁽²⁾	410.248 ⁽²⁾	410.248 ⁽²⁾
0.02		436.849 ⁽²⁾	446.944 ⁽²⁾	490.081 ⁽²⁾	500.240 ⁽²⁾	462.020 ⁽²⁾	472.178 ⁽²⁾
0.04		489.332 ⁽²⁾	509.721 ⁽²⁾	547.575 ⁽²⁾	567.953 ⁽²⁾	516.913 ⁽²⁾	537.362 ⁽²⁾
0.06		544.684 ⁽²⁾	575.523 ⁽²⁾	607.901 ⁽²⁾	638.518 ⁽²⁾	574.668 ⁽²⁾	605.496 ⁽²⁾
0.08		602.898 ⁽²⁾	644.302 ⁽²⁾	671.043 ⁽²⁾	711.871 ⁽²⁾	635.265 ⁽²⁾	676.526 ⁽²⁾
0.10		663.969 ⁽²⁾	716.005 ⁽²⁾	736.962 ⁽²⁾	787.941 ⁽²⁾	698.696 ⁽²⁾	750.389 ⁽²⁾
0.12		727.866 ⁽²⁾	790.572 ⁽²⁾	805.623 ⁽²⁾	866.656 ⁽²⁾	764.918 ⁽²⁾	827.015 ⁽²⁾
0.14		794.572 ⁽²⁾	867.937 ⁽²⁾	876.983 ⁽²⁾	947.938 ⁽²⁾	833.895 ⁽²⁾	906.334 ⁽²⁾
0.16		864.047 ⁽²⁾	948.027 ⁽²⁾	950.996 ⁽²⁾	1031.706 ⁽²⁾	905.605 ⁽²⁾	988.268 ⁽²⁾
0.18		936.251 ⁽²⁾	1030.767 ⁽²⁾	1027.611 ⁽²⁾	1117.880 ⁽²⁾	979.976 ⁽²⁾	1072.737 ⁽²⁾
0.20		1011.143 ⁽²⁾	1116.077 ⁽²⁾	1106.773 ⁽²⁾	1206.373 ⁽²⁾	1056.990 ⁽²⁾	1159.658 ⁽²⁾
0.22		1088.685 ⁽²⁾	1203.874 ⁽²⁾	1188.427 ⁽²⁾	1297.100 ⁽²⁾	1136.575 ⁽²⁾	1248.945 ⁽²⁾
0.24		1168.822 ⁽²⁾	1294.071 ⁽²⁾	1272.512 ⁽²⁾	1389.973 ⁽²⁾	1218.669 ⁽²⁾	1340.511 ⁽²⁾
0.26		1251.494 ⁽²⁾	1386.578 ⁽²⁾	1358.961 ⁽²⁾	1482.798 ⁽³⁾	1303.240 ⁽²⁾	1434.266 ⁽²⁾
0.28		1336.646 ⁽²⁾	1481.305 ⁽²⁾	1447.729 ⁽²⁾	1570.785 ⁽³⁾	1390.203 ⁽²⁾	1530.119 ⁽²⁾
0.30		1424.221 ⁽²⁾	1578.159 ⁽²⁾	1538.729 ⁽²⁾	1659.676 ⁽³⁾	1479.504 ⁽²⁾	1627.977 ⁽²⁾
0.32		1514.154 ⁽²⁾	1677.046 ⁽²⁾	1631.914 ⁽²⁾	1749.368 ⁽³⁾	1571.078 ⁽²⁾	1727.749 ⁽²⁾
0.34		1606.368 ⁽²⁾	1777.871 ⁽²⁾	1727.204 ⁽²⁾	1839.757 ⁽³⁾	1664.859 ⁽²⁾	1829.341 ⁽²⁾
0.36		1700.842 ⁽²⁾	1880.538 ⁽²⁾	1818.429 ⁽³⁾	1930.746 ⁽³⁾	1760.780 ⁽²⁾	1921.489 ⁽³⁾
0.38		1797.464 ⁽²⁾	1984.951 ⁽²⁾	1908.555 ⁽³⁾	2022.236 ⁽³⁾	1858.770 ⁽²⁾	2013.090 ⁽³⁾
0.40		1896.181 ⁽²⁾	2091.014 ⁽²⁾	1999.754 ⁽³⁾	2114.133 ⁽³⁾	1958.773 ⁽²⁾	2105.115 ⁽³⁾
0.42		1996.925 ⁽²⁾	2188.758 ⁽³⁾	2091.963 ⁽³⁾	2206.347 ⁽³⁾	2060.708 ⁽²⁾	2197.472 ⁽³⁾
0.44		2099.626 ⁽²⁾	2281.500 ⁽³⁾	2185.102 ⁽³⁾	2298.789 ⁽³⁾	2164.510 ⁽²⁾	2290.070 ⁽³⁾
0.46		2204.206 ⁽²⁾	2374.408 ⁽³⁾	2279.104 ⁽³⁾	2391.374 ⁽³⁾	2266.625 ⁽³⁾	2382.821 ⁽³⁾
0.48		2310.623 ⁽²⁾	2467.396 ⁽³⁾	2373.903 ⁽³⁾	2484.019 ⁽³⁾	2361.442 ⁽³⁾	2475.644 ⁽³⁾
0.50		2418.780 ⁽²⁾	2560.384 ⁽³⁾	2469.411 ⁽³⁾	2576.645 ⁽³⁾	2457.007 ⁽³⁾	2568.455 ⁽³⁾

$$\bar{P} = \frac{P_{cr} a^2}{\Upsilon_1} \quad (31)$$

where Υ_1 has been defined in Appendix A as Eqs. (A.3) and (A.7) for closed and open circuit conditions, respectively.

The effect of the aspect ratio on the non-dimensional critical buckling load of a plate under different boundary conditions is presented in Figs. 11 and 12. Fig. 11 corresponds to the SCSC, SCSS and SSSS boundary conditions and Fig. 12 corresponds to SFSF, SFSC and SFSS boundary conditions. In these figures, the non-dimensional critical buckling load versus aspect ratio is plotted for a plate under biaxial compression. As these figures show, for all boundary conditions except SFSF, the non-dimensional critical buckling load decreases as aspect ratio increases.

By comparing Figs. 11 and 12, it can be observed that for all boundary conditions, the non-dimensional critical buckling load is nearly constant for high aspect ratios, which means, for high aspect ratios, the effect of boundary condition on the critical buckling load is negligible.

In Tables 5 and 6, the critical buckling loads of plate under both closed and open circuit electrical conditions and different mechanical boundary conditions are presented for $a/b=0.5$ and 1, respectively. It can be seen that the critical buckling load for closed circuit piezoelectric layer is less than open one regardless of mechanical boundary conditions and also for both electrical boundary condition, the lowest and highest of the critical boundary condition are related to SFSF and SCSC, respectively, as predicted.

It should be noted that the critical buckling load which is the lowest buckling load, may not occur in the first mode, therefore, in Tables 7 and 8 for various mechanical boundary conditions, the mode numbers are presented for the cases that it is different for open and closed circuit conditions. These tables indicate that h_p can increase the mode number. Furthermore, the mode number in open circuit piezoelectric layer is always equal to or greater than that of closed one. It may be concluded that changing the electrical boundary condition can change the mode number. Furthermore, in Table 9 the critical buckling load for isotropic and transversely isotropic materials are presented. As mentioned, the critical buckling load for

Table 8 The critical buckling load and mode number of a simply supported square plate subjected to biaxial compression and tension

$2h/a$	0.05		0.08		0.1	
	Closed	Open	Closed	Open	closed	Open
0	60.519 ⁽²⁾	60.519 ⁽²⁾	219.391 ⁽²⁾	219.391 ⁽²⁾	387.471 ⁽²⁾	387.471 ⁽²⁾
0.02	68.637 ⁽²⁾	65.453 ⁽²⁾	248.002 ⁽²⁾	236.535 ⁽²⁾	436.849 ⁽²⁾	446.944 ⁽²⁾
0.04	77.434 ⁽²⁾	70.644 ⁽²⁾	278.633 ⁽²⁾	254.374 ⁽²⁾	489.332 ⁽²⁾	509.721 ⁽²⁾
0.06	86.846 ⁽²⁾	81.568 ⁽²⁾	311.144 ⁽²⁾	291.615 ⁽²⁾	544.684 ⁽²⁾	575.523 ⁽²⁾
0.08	96.891 ⁽²⁾	93.228 ⁽²⁾	345.544 ⁽²⁾	330.944 ⁽²⁾	602.898 ⁽²⁾	644.302 ⁽²⁾
0.10	107.584 ⁽²⁾	105.640 ⁽²⁾	381.849 ⁽²⁾	372.362 ⁽²⁾	663.969 ⁽²⁾	716.005 ⁽²⁾
0.12	118.942 ⁽²⁾	118.817 ⁽²⁾	420.076 ⁽²⁾	415.863 ⁽²⁾	727.866 ⁽²⁾	790.572 ⁽²⁾
0.14	130.975 ⁽²⁾	132.773 ⁽²⁾	460.220 ⁽²⁾	461.437 ⁽²⁾	794.572 ⁽²⁾	867.937 ⁽²⁾
0.16	143.698 ⁽²⁾	147.519 ⁽²⁾	502.296 ⁽²⁾	509.070 ⁽²⁾	864.047 ⁽²⁾	948.027 ⁽²⁾
0.18	157.121 ⁽²⁾	163.066 ⁽²⁾	546.293 ⁽²⁾	558.745 ⁽²⁾	936.251 ⁽²⁾	1030.767 ⁽²⁾
0.20	171.260 ⁽²⁾	179.424 ⁽²⁾	592.212 ⁽²⁾	610.440 ⁽²⁾	1011.143 ⁽²⁾	1116.077 ⁽²⁾
0.22	186.124 ⁽²⁾	196.602 ⁽²⁾	640.055 ⁽²⁾	664.130 ⁽²⁾	1088.685 ⁽²⁾	1203.874 ⁽²⁾
0.24	201.718 ⁽²⁾	214.608 ⁽²⁾	689.793 ⁽²⁾	719.785 ⁽²⁾	1168.822 ⁽²⁾	1294.071 ⁽²⁾
0.26	218.061 ⁽²⁾	233.449 ⁽²⁾	741.425 ⁽²⁾	777.376 ⁽²⁾	1251.494 ⁽²⁾	1386.578 ⁽²⁾
0.28	235.152 ⁽²⁾	253.131 ⁽²⁾	794.925 ⁽²⁾	836.867 ⁽²⁾	1336.646 ⁽²⁾	1481.305 ⁽²⁾
0.30	253.005 ⁽²⁾	273.658 ⁽²⁾	850.291 ⁽²⁾	898.222 ⁽²⁾	1424.221 ⁽²⁾	1578.159 ⁽²⁾
0.32	271.625 ⁽²⁾	295.036 ⁽²⁾	907.483 ⁽²⁾	961.401 ⁽²⁾	1514.154 ⁽²⁾	1677.046 ⁽²⁾
0.34	291.017 ⁽²⁾	317.266 ⁽²⁾	966.495 ⁽²⁾	1026.363 ⁽²⁾	1606.368 ⁽²⁾	1777.871 ⁽²⁾
0.36	311.187 ⁽²⁾	340.352 ⁽²⁾	1027.293 ⁽²⁾	1093.066 ⁽²⁾	1700.842 ⁽²⁾	1880.538 ⁽²⁾
0.38	332.141 ⁽²⁾	364.295 ⁽²⁾	1089.851 ⁽²⁾	1161.463 ⁽²⁾	1797.464 ⁽²⁾	1984.951 ⁽²⁾
0.40	353.878 ⁽²⁾	389.095 ⁽²⁾	1154.135 ⁽²⁾	1231.509 ⁽²⁾	1896.181 ⁽²⁾	2091.014 ⁽²⁾
0.42	376.415 ⁽²⁾	414.752 ⁽²⁾	1220.136 ⁽²⁾	1303.155 ⁽²⁾	1996.925 ⁽²⁾	2188.758 ⁽³⁾
0.44	399.736 ⁽²⁾	441.265 ⁽²⁾	1287.790 ⁽²⁾	1376.352 ⁽²⁾	2099.626 ⁽²⁾	2281.500 ⁽³⁾
0.46	423.863 ⁽²⁾	468.632 ⁽²⁾	1357.107 ⁽²⁾	1451.051 ⁽²⁾	2204.206 ⁽²⁾	2374.408 ⁽³⁾
0.48	448.782 ⁽²⁾	496.851 ⁽²⁾	1428.018 ⁽²⁾	1527.199 ⁽²⁾	2310.623 ⁽²⁾	2467.396 ⁽³⁾
0.50	474.500 ⁽²⁾	525.918 ⁽²⁾	1500.492 ⁽²⁾	1604.746 ⁽²⁾	2418.780 ⁽²⁾	2560.384 ⁽³⁾

Table 9 The critical buckling loads of isotropic and transversely isotropic plates under different boundary and loading conditions for open and closed circuit ($a/b=1, h_p/2h=0.5$)

R	Boundary condition							
			SCSC	SCSS	SSSS	SFSC	SFSS	SFSF
1	Closed	isotropic	1352.077	1078.989	891.923	519.086	494.326	457.936
		transversely	1161.612	958.225	813.669	484.415	464.332	435.253
	Open	isotropic	1519.112	1236.447	1038.463	534.543	513.932	491.910
		transversely	1272.223	1073.166	928.989	495.461	478.871	463.405
0	Closed	isotropic	2301.513 ⁽²⁾	2213.788 ⁽²⁾	1784.179	757.173	673.173	472.3956
		transversely	1914.809 ⁽²⁾	1861.547 ⁽²⁾	1629.745	705.295	635.117	449.823
	Open	isotropic	2534.168 ⁽²⁾	2456.747 ⁽²⁾	2077.763	818.317	737.632	527.851
		transversely	2061.899 ⁽²⁾	2019.553 ⁽²⁾	1864.162	756.376	690.641	498.954
-1	Closed	isotropic	3078.651 ⁽²⁾	2959.909 ⁽²⁾	2849.099 ⁽²⁾	1095.342	932.341	477.682
		transversely	2469.410 ⁽³⁾	2457.007 ⁽³⁾	2418.780 ⁽²⁾	1007.937	877.614	454.639
	Open	isotropic	3330.528 ⁽³⁾	3280.915 ⁽²⁾	3183.308 ⁽²⁾	1218.402	1050.659	541.712
		transversely	2576.645 ⁽³⁾	2568.455 ⁽³⁾	2560.384 ⁽³⁾	1106.721	978.328	511.193

isotropic material is larger than that of transversely isotropic one.

8. Conclusions

In the present article, an analytical method has been developed for buckling analysis of transversely isotropic rectangular plates with surface bonded piezoelectric layers. Based on the first-order shear deformation plate theory (FSDT) the stability and equilibrium equations have been derived. Four coupled stability equations have been decoupled using some analytical functions. The critical buckling loads for Levy type of mechanical boundary conditions and closed and open circuit electrical boundary conditions are presented. From the numerical results the following conclusions can be remarked:

- 1- The electrical effect of piezoelectric layer increases the buckling load for both open and closed circuit conditions.
- 2- Changing the closed circuit condition to open one can increase the buckling mode number.
- 3- Changing core material from transversely isotropic to isotropic increases the critical buckling loads.
- 4- The highest and lowest values for the critical buckling load in all electrical and mechanical boundary conditions are related to the plates under biaxial compression, and tension and biaxial compression, respectively.
- 5- The effect of variation in reduced stiffness matrix on the critical buckling load is more noticeable than other piezoelectric properties.
- 6- For all Levy boundary conditions, except SFSF, increasing the aspect ratio decreases the nondimensional critical buckling load.

References

- Abdollahi, M., Saidi, A. and Mohammadi, M. (2015), "Buckling analysis of thick functionally graded piezoelectric plates based on the higher-order shear and normal deformable theory", *Acta Mechanica* **226**(8), 1-14.
- Akhras, G. and Li, W. (2010), "Three-dimensional thermal buckling analysis of piezoelectric antisymmetric angle-ply laminates using finite layer method", *Compos. Struct.*, **92**(1), 31-38.
- Arefi, M. (2016), "Buckling analysis of the functionally graded sandwich rectangular plates integrated with piezoelectric layers under bi-axial loads", *J. Sandwich Struct. Mater.*, doi: 10.1177/1099636216642393.
- Askari Farsangi, M.A. and Saidi, A. (2012), "Levy type solution for free vibration analysis of functionally graded rectangular plates with piezoelectric layers", *Smart Mater. Struct.*, **21**(9), 1-15.
- Askari Farsangi, M.A., Saidi, A. and Batra, R. (2013), "Analytical solution for free vibrations of moderately thick hybrid piezoelectric laminated plates", *J. Sound Vib.*, **332**(22), 5981-5998.
- Batra, R. and Geng, T. (2001a), "Enhancement of the dynamic buckling load for a plate by using piezoceramic actuators", *Smart Mater. Struct.*, **10**(5), 925-933.
- Bodaghi, M. and Saidi, A. (2010), "Levy-type solution for buckling analysis of thick functionally graded rectangular plates based on the higher-order shear deformation plate theory", *Appl. Math. Model.*, **34**(11), 3659-3673.
- Bodaghi, M. and Saidi, A. (2011a), "Buckling behavior of standing laminated Mindlin plates subjected to body force and vertical loading", *Compos. Struct.*, **93**(2), 538-547.
- Bodaghi, M. and Saidi, A. (2011b), "Thermoelastic buckling behavior of thick functionally graded rectangular plates", *Arch. Appl. Mech.*, **81**(11), 1555-1572.
- Chandrashekhara, K. and Bhatia, K. (1993), "Active buckling control of smart composite plates-finite-element analysis", *Smart Mater. Struct.*, **2**(1), 31-38.
- Chen, X.L., Zhao, Z.Y. and Liew, K.M. (2008), "Stability of piezoelectric FGM rectangular plates subjected to non-uniformly distributed load, heat and voltage", *Adv. Eng. Softw.*, **39**(2), 121-131.
- Cheng, J., Han, H. and Taheri, F. (2008), "An adaptive enhancement of dynamic buckling of a laminated composite beam under axial impact by surface bonded piezoelectric patches", *Comput. Method. Appl. Mech. Eng.*, **197**(33), 2680-2691.
- De Faria, A. (2004), "On buckling enhancement of laminated beams with piezoelectric actuators via stress stiffening", *Compos. Struct.*, **65**(2), 187-192.
- De Faria, A.R. and De Almeida, S.F.M. (1999), "Enhancement of pre-buckling behavior of composite beams with geometric imperfections using piezoelectric actuators", *Compos. Part B: Eng.*, **30**(1), 43-50.
- Faria, A.R.D. and Donadon, M.V. (2010), "The use of piezoelectric stress stiffening to enhance buckling of laminated plates", *Latin Am. J. Solid. Struct.*, **7**(2), 167-183.
- Giannopoulos, G., Santafe, F., Monreal, J. and Vantomme, J. (2007), "Thermal, electrical, mechanical coupled mechanics for initial buckling analysis of smart plates and beams using discrete layer kinematics", *Int. J. Solid. Struct.*, **44**(14), 4707-4722.
- Jadhav, P.A. and Bajoria, K.M. (2012), "Buckling of piezoelectric functionally graded plate subjected to electro-mechanical loading", *Smart Mater. Struct.*, **21**(10), 1-10.
- Jerome, R. and Ganesan, N. (2010), "New generalized plane strain FE formulation for the buckling analysis of piezocomposite beam", *Finite Element. Anal. Des.*, **46**(10), 896-904.
- Jomehzadeh, E. and Saidi, A. (2009), "Analytical solution for free vibration of transversely isotropic sector plates using a boundary layer function", *Thin-Wall. Struct.*, **47**(1), 82-88.
- Kapurja, S. and Achary, G. (2004), "Exact 3-D piezoelectricity solution for buckling of hybrid cross-ply plates using transfer matrices", *Acta Mechanica*, **170**(1-2), 25-45.
- Kapurja, S. and Achary, G. (2006), "Nonlinear coupled zigzag theory for buckling of hybrid piezoelectric plates", *Compos. Struct.*, **74**(3), 253-264.
- Kapurja, S. and Alam, N. (2004a), "Exact two-dimensional piezoelectricity solution for buckling of hybrid beams and cross-ply panels using transfer matrices", *Compos. Struct.*, **64**(1), 1-11.
- Kapurja, S. and Alam, N. (2004b), "Zigzag theory for buckling of hybrid piezoelectric beams under electromechanical loads", *Int. J. Mech. Sci.*, **46**(1), 1-25.
- Kim, G.W. and Lee, K.Y. (2008), "Influence of weak interfaces on buckling of orthotropic piezoelectric rectangular laminates", *Compos. Struct.*, **82**(2), 290-294.
- Lei, Z.X., Zhang, L.W. and Liew, K.M. (2016), "Buckling analysis of CNT reinforced functionally graded laminated composite plates", *Compos. Struct.*, **152**, 62-73.
- Liew, K.M., Yang, J. and Kitipornchai, S. (2003), "Postbuckling of piezoelectric FGM plates subject to thermo-electro-mechanical loading", *Int. J. Solid. Struct.*, **40**(15), 3869-3892.

- Mirzavand, B. and Eslami, M. (2011), "A closed-form solution for thermal buckling of piezoelectric FGM rectangular plates with temperature-dependent properties", *Acta Mechanica*, **218**(1-2), 87-101.
- Mohammadi, M., Saidi, A. and Jomehzadeh, E. (2010), "A novel analytical approach for the buckling analysis of moderately thick functionally graded rectangular plates with two simply-supported opposite edges", *Proc. Inst. Mech. Engineers, Part C: J. Mech. Eng. Sci.*, **224**(9), 1831-1841.
- Oh, I., Han, J. and Lee, I. (2000), "Postbuckling and vibration characteristics of piezolaminated composite plate subject to thermo-piezoelectric loads", *J. Sound Vib.*, **233**(1), 19-40.
- Rahmat Talabi, M.R. and Saidi, A. (2013), "An explicit exact analytical approach for free vibration of circular/annular functionally graded plates bonded to piezoelectric actuator/sensor layers based on Reddy's plate theory", *Appl. Math. Model.*, **37**(14), 7664-7684.
- Saidi, A. and Jomehzadeh, E. (2009), "On the analytical approach for the bending/stretching of linearly elastic functionally graded rectangular plates with two opposite edges simply supported", *Proc. Inst. Mech. Engineers, Part C: J. Mech. Eng. Sci.*, **223**(9), 2009-2016.
- Shariyat, M. (2009a), "Dynamic buckling of imperfect laminated plates with piezoelectric sensors and actuators subjected to thermo-electro-mechanical loadings, considering the temperature-dependency of the material properties", *Compos. Struct.*, **88**(2), 228-239.
- Shariyat, M. (2009b), "Vibration and dynamic buckling control of imperfect hybrid FGM plates with temperature-dependent material properties subjected to thermo-electro-mechanical loading conditions", *Compos. Struct.*, **88**(2), 240-252.
- Shen, H.S. (2001a), "Postbuckling of shear deformable laminated plates with piezoelectric actuators under complex loading conditions", *Int. J. Solid. Struct.*, **38**(44), 7703-7721.
- Shen, H.S. (2001b), "Thermal postbuckling of shear-deformable laminated plates with piezoelectric actuators", *Compos. Sci. Technol.*, **61**(13), 1931-1943.
- Shen, H.S. (2005), "Postbuckling of FGM plates with piezoelectric actuators under thermo-electro-mechanical loadings", *Int. J. Solid. Struct.*, **42**(23), 6101-6121.
- Shen, H.S. (2009), "A comparison of buckling and postbuckling behavior of FGM plates with piezoelectric fiber reinforced composite actuators", *Compos. Struct.*, **91**(3), 375-384.
- Thai, H., Nguyen, T., Vo, T.P. and Lee, J. (2014), "Analysis of functionally graded sandwich plates using a new first-order shear deformation theory", *Eur. J. Mech. A/Solid.*, **45**, 211-225.
- Thang, P.T. (2016), "Analytical solution for thermal buckling analysis of rectangular plates with functionally graded coatings", *Aero. Sci. Technol.*, **55**, 465-473.
- Varelis, D. and Saravanos, D.A. (2002), "Nonlinear coupled mechanics and initial buckling of composite plates with piezoelectric actuators and sensors", *Smart Mater. Struct.*, **11**(3), 330-336.
- Varelis, D. and Saravanos, D.A. (2004), "Coupled buckling and postbuckling analysis of active laminated piezoelectric composite plates", *Int. J. Solid. Struct.*, **41**(5), 1519-1538.
- Wang, Q. (2002), "On buckling of column structures with a pair of piezoelectric layers", *Eng. Struct.*, **24**(2), 199-205.
- Wang, Q. (2010), "Active buckling control of beams using piezoelectric actuators and strain gauge sensors", *Smart Mater. Struct.*, **19**(6), 065022.
- Wang, Q. and Quek, S. (2002), "Enhancing flutter and buckling capacity of column by piezoelectric layers", *Int. J. Solid. Struct.*, **39**(16), 4167-4180.
- Wang, Q., Quek, S., Sun, C. and Liu, X. (2001), "Analysis of piezoelectric coupled circular plate", *Smart Mater. Struct.*, **10**(2), 229-239.
- Wu, N., Wang, Q. and Quek, S. (2010), "Free vibration analysis of piezoelectric coupled circular plate with open circuit", *J. Sound Vib.*, **329**(8), 1126-1136.
- Yaghoobi, H. and Rajabi, I. (2013), "Buckling analysis of three-layered rectangular plate with piezoelectric layers", *J. Theo. Appl. Mech.*, **51**, 813-826.

CC

Appendix A

The components of reduced stiffness matrix at constant electric field and the reduced matrix of piezoelectric electric constants can be written as

$$\bar{C}_{11}^E = C_{11}^E - \frac{C_{13}^E}{C_{33}^E}, \bar{C}_{12}^E = C_{12}^E - \frac{C_{13}^E}{C_{33}^E}, \bar{e}_{31} = e_{31} - \frac{C_{13}^E}{C_{33}^E} e_{33}, \bar{\epsilon}_{33} = \epsilon_{33} + \frac{e_{33}^2}{C_{33}^E} \quad (\text{A.1})$$

Coefficients in Eqs. (12) through (18) are listed as

(a) Closed circuit condition

$$F_1 = \int_{-h}^h \frac{E}{1-\nu^2} dz + 2 \int_h^{h+h_p} \bar{C}_{11}^E dz \quad (\text{A.2})$$

$$F_2 = \int_{-h}^h \frac{\nu E}{1-\nu^2} dz + 2 \int_h^{h+h_p} \bar{C}_{12}^E dz$$

$$Y_1 = \int_{-h}^h \frac{E}{1-\nu^2} z^2 dz + 2 \int_h^{h+h_p} \bar{C}_{11}^E z^2 dz$$

$$Y_2 = \int_{-h}^h \frac{E}{2(1+\nu)} z^2 dz + 2 \int_h^{h+h_p} \frac{1}{2} (\bar{C}_{11}^E - \bar{C}_{12}^E) z^2 dz \quad (\text{A.3})$$

$$Y_3 = \int_{-h}^h \frac{\nu E}{1-\nu^2} z^2 dz + 2 \int_h^{h+h_p} \bar{C}_{12}^E z^2 dz$$

$$\Theta_1 = 2 \int_h^{h+h_p} \bar{e}_{31} \left(-\frac{8(z-h-h_p/2)}{h_p^2} \right) z dz$$

$$\Theta_2 = 2 \int_h^{h+h_p} \bar{e}_{15} \left(1 - \frac{4(z-h-h_p/2)^2}{h_p^2} \right) dz \quad (\text{A.4})$$

$$\Theta_3 = 0$$

$$\eta_1 = (\bar{e}_{15} + \bar{e}_{31}) h_p \quad \eta_2 = h_p \bar{e}_{15} \quad \eta_3 = 0$$

$$\eta_4 = \frac{8\bar{\epsilon}_{33}}{h_p} \quad \eta_5 = -\frac{2\bar{\epsilon}_{11} h_p}{3} \quad (\text{A.5})$$

(b) Open circuit condition

$$F_1 = \int_{-h}^h \frac{E}{1-\nu^2} dz + 2 \int_h^{h+h_p} \bar{C}_{11}^E dz \quad (\text{A.6})$$

$$F_2 = \int_{-h}^h \frac{\nu E}{1-\nu^2} dz + 2 \int_h^{h+h_p} \bar{C}_{12}^E dz$$

$$Y_1 = \int_{-h}^h \frac{E}{1-\nu^2} z^2 dz + 2 \int_h^{h+h_p} \bar{C}_{11}^E z^2 dz$$

$$Y_2 = \int_{-h}^h \frac{E}{2(1+\nu)} z^2 dz + 2 \int_h^{h+h_p} \frac{1}{2} (\bar{C}_{11}^E - \bar{C}_{12}^E) z^2 dz \quad (\text{A.7})$$

$$Y_3 = \int_{-h}^h \frac{\nu E}{1-\nu^2} z^2 dz + 2 \int_h^{h+h_p} \bar{C}_{12}^E z^2 dz$$

$$\Theta_1 = 2 \int_h^{h+h_p} \bar{e}_{31} \left(-\frac{8(z-h-h_p/2)}{h_p^2} + \frac{4}{h_p} \right) z dz$$

$$\Theta_2 = 2 \int_h^{h+h_p} \bar{e}_{15} \left(1 - \frac{4(z-h-h_p/2)^2}{h_p^2} + \frac{4}{h_p} (z-h) \right) dz \quad (\text{A.8})$$

$$\Theta_3 = 2 \int_h^{h+h_p} \frac{\bar{e}_{15} \bar{e}_{31}}{\bar{\epsilon}_{33}} (h+h_p) (z-h) dz$$

$$\eta_1 = (\bar{e}_{15} + \bar{e}_{31}) h_p \quad \eta_2 = h_p \bar{e}_{15} \quad \eta_3 = -\frac{\bar{\epsilon}_{11} \bar{e}_{31} h_p^2}{2\bar{\epsilon}_{33}} (h+h_p)$$

$$\eta_4 = \frac{8\bar{\epsilon}_{33}}{h_p} \quad \eta_5 = -\frac{8\bar{\epsilon}_{11} h_p}{3} \quad (\text{A.9})$$

Appendix B

Coefficients in Eq. (22) are as follow

$$\Omega_2 = \Theta_1 - \Theta_2$$

$$\Omega_1 = Y_1 - \Theta_3$$

$$m_1 = -\frac{\Omega_1 j_4 k_2 - \Omega_2 j_3 k_2}{j_4 k_1}$$

$$m_2 = -\frac{\Omega_1 j_4 k_3 + \Omega_2 j_2 k_1 - \Omega_2 j_3 k_3 - C j_4 k_2}{j_4 k_1}$$

$$m_3 = -\frac{C j_4 k_3 + C j_4 k_1}{j_4 k_1}$$

$$m_4 = -\frac{\Omega_1 j_4 k_5 - \Omega_2 j_3 k_5}{j_4 k_1}$$

$$m_5 = -\frac{\Omega_1 j_4 k_4 + \Omega_2 j_1 k_1 - \Omega_2 j_3 k_4 - C j_4 k_5}{j_4 k_1} \quad (\text{B.1})$$

$$m_6 = \frac{C k_4}{k_1}$$

$$k_1 = \frac{\Theta_2 j_3 g_2 + C j_4 g_3 - \Theta_3 j_4 g_2}{j_4 g_3}$$

$$k_2 = -\frac{\Theta_2 j_2}{j_4}$$

$$k_3 = \frac{\Theta_2 j_3 g_1 + C j_4 g_3 - \Theta_3 j_4 g_1}{j_4 g_3}$$

$$k_4 = \frac{\Theta_2 j_3 - \Theta_3 j_4 + j_4 g_3}{j_4 g_3}$$

$$k_5 = -\frac{\Theta_2 j_1}{j_4}$$

$$j_1 = \frac{\eta_5 g_3 h_3 - \eta_3}{g_3}$$

$$j_2 = \frac{\eta_2 g_3 - \eta_3 g_1 + \eta_5 g_3 h_2}{g_3}$$

$$j_3 = \frac{\eta_5 g_3 h_1 - \eta_3 g_2 + \eta_1 g_3}{g_3}$$

$$j_4 = \eta_4$$

$$h_1 = \frac{\Omega_1 g_2 + C g_3}{g_3 \Omega_2}$$

$$h_2 = \frac{\Omega_1 g_1 + C g_3}{g_3 \Omega_2}$$

$$h_3 = \frac{\Omega_1}{g_3 \Omega_2}$$

$$g_1 = g_2 = \frac{\Theta_2 C + \Omega_2 C}{\Omega_2}$$

$$g_3 = -\frac{-\Theta_2 \Omega_2 + \Theta_2 \Omega_1}{\Omega_2}$$

$$\lambda_4 = \frac{\sqrt{d_8 \beta^2 - d_6}}{\sqrt{d_8}}$$